Immunoproteasomes in Microglial Activation and Inflammation

Katiuska Daniela Pulgar Prieto

Imperial College London

Department of Medicine

Primary Supervisor: Dr Yu Ye

Secondary Supervisor: Dr David Thomas

Thesis Submitted for the Degree of MPhil in Clinical Medicine Research

Abstract

Chronic neuroinflammation and aggregation of misfolded proteins, like tau or α-synuclein, are distinctive features of neurodegenerative disorders. The ubiquitin-proteasome system (UPS) has been shown to be directly involved in the degradation of aggregates, as well as in sustaining inflammation in Alzheimer's disease. Pro-inflammatory stimuli, such as cytokines, are known to upregulate proteasomal subunits which presumably lead to enhanced degradation. However, the exact role of the UPS in regulating inflammatory responses is not well understood.

This MPhil project mainly focuses on the underlying mechanisms of the UPS in microglia, which are suspected to lead to chronic inflammation in neurodegenerative disorders. I am especially interested in the distinct functions of the standard (sP) versus the immuno-proteasome (iP) in regulating pro-inflammatory signaling in the NF-kB and c/EBPb pathways. I performed advanced fluorescence imaging on iPSC-derived microglia stimulated with TNF-α, IFN-γ or LPS. Intriguingly, my preliminary results in microglia suggested that both the sP and the iP are upregulated upon stimulation, with different localization patterns. This indicates that the sPs and iPs may carry out distinct roles in response to external stimuli. I further tested how proteasomes responded to aggregate stimuli in cell lines already established in our lab, and found that proteasomes accumulated around invading aggregates, forming foci in a cytoskeleton-dependent manner. The next stage of this research would be to study sPs and iPs in microglia differentiated from patient-derived iPSCs, and how their relative ratio and activities regulate distinct inflammatory pathways. Revealing the individual functions of the sPs versus the iPs will unveil novel targets for therapeutic intervention against overactive microglia.

Table of Contents

ABSTRACT **2**

LIST OF FIGURES AND TABLES **5**

STATEMENT OF ORIGINALITY **6**

COPYRIGHT STATEMENT **7**

1. INTRODUCTION **8**

1.1 Inflammation in Neurodegenerative Diseases **8**

1.2 Ubiquitin-Proteasome System **9**

1.3 Project Aims and Hypotheses **11**

2. METHODS **12**

2.1 Cloning **12**

2.2 Cells and Culture Conditions **13**

2.3 Cell Line Manipulations **13**

2.4 Establishing Cell Lines **14**

2.5 Native Gel Electrophoresis **14**

2.6 α-Synuclein Aggregation **15**

2.7 Immunocytochemistry **15**

2.8 RNA Extraction **16**

2.9 Microscopy **16**

3. UNDERSTANDING PROTEASOME FOCI FORMATION **17**

3.1 Results and Discussion **17**

3.1.1 Aggregate-Stress Induced Foci are not Liquid-Liquid Phase Separated 17

3.1.2 Cytoskeleton Aids in Aggregate Stress-Induced Foci Formation 19

3.2 Conclusion **19**

4. DECIPHERING THE MECHANISM BY WHICH IMMUNOPROTEASOMES MODULATE MICROGLIA ACTIVATION 21

4.1 Results and Discussion 21
4.1.1 Fluorescently Tagged Proteasome Subunits Incorporate into the Endogenous Proteasome Complex 21
4.1.2 Knocking-in FPs in LN229 22
4.1.3 Knock-out of Endogenous $h\beta_5$ or $h\beta_{5i}$ in LN229 24
4.1.4 Proteasome Expression Levels Increase under Inflammatory Stress 24
4.1.5 Establishing a Proteasome Degradation Assay: Ub^{G76V}-Dendra2 25

4.2 Future Studies 29

5. FUTURE WORK……. 31

BIBLIOGRAPHY 34

APPENDIX 41

List of Figures and Tables

Figure 1. Standard 26S proteasome 9

Figure 2. CP of sP versus iP 10

Table 1. gRNA from CRISPR editing 12

Table 2. Antibodies for Immunocytochemistry 15

Figure 3. Aggregate-induced foci are not liquid-liquid phase separated 18

Figure 4. Osmotic stress-induced foci are not cytoskeleton dependent 19

Figure 5. Cloning fluorescent tags onto proteasome subunits 20

Figure 6. mEos4b knock-ins 22

Figure 7. Colony #11 and #55 have mEos4b inserted downstream of PSMB8 23

Figure 8. Inflammatory stress for 24 hours upregulates β_5 and β_{5i} subunits 25

Figure 9. Inflammatory stress for 72 hours upregulates β_5 and β_{5i} subunits 26

Figure 10. Schematic representation of Ub^{G76V}-Dendra2 27

Figure 11. Selecting LN229-Ub^{G76V}-Dendra2 clones 28

Figure 12. qPCR targets of inflammation 30

Appendix Figure A1. Map of pcsII-hβ_5-FP 37

Appendix Figure A2. Map of pcsII-hβ_{5i}-FP 38

Appendix Figure A3. Map of Cas9 plasmid 39

Statement of Originality

I certify the sole authorship of this thesis and that, to the best of my knowledge, it does not violate any proprietary rights. Any material from the work of others included in my thesis are fully acknowledged and referenced appropriately. This thesis has not been submitted elsewhere for publication or other purposes.

Copyright Statement

1. Introduction

1.1 Inflammation in Neurodegenerative Diseases

Neurodegenerative disorders are a group of debilitating conditions where neuronal functions are compromised[1]. For instance, Alzheimer's disease (AD) is associated with neuronal loss in the hippocampus and cerebral cortex leading to cognitive decline[2], while Parkinson's disease (PD) is connected to movement disorders originated in death of dopaminergic neurons in the substantia nigra[3]. Current treatments for AD and PD mainly focus on relieving symptoms in expectation of a future cure to reverse neuronal degeneration. There is therefore an urgency to characterize the underlying mechanisms that drive these pathologies to find therapeutic interventions that target this group of disorders.

A common feature of neurodegenerative disorders is the pathogenic accumulation of aggregates such as neurofibrillary tangles and Lewy bodies, formed from misfolded proteins of tau or α-synuclein (αSyn) respectively[4]. For a long time, the large filamentous aggregates (fibrils) were generally believed to be the culprits of neurodegeneration. However, increasing data from recent years have demonstrated that it is the mechanisms of smaller aggregates such as the soluble oligomers, which efficiently penetrate membranes, inducing stress responses and blocking proteostasis[5,6]. Aggregated species have been found inside neurons, disrupting their signalling capabilities[7,8]. Furthermore, it has been shown that neurons release α-Synuclein aggregates into the extracellular space, acting as a chemoattractant to microglia which over-activate it, causing the release of pro-inflammatory cytokines such as IL-6, IL1-β, and TNF-α, fostering an inflammatory environment[9-11]. Neuronal health is regulated by microglia, the immune cells of the brain that provide surveillance, by engulfing and degrading the neurons that are severely damaged. Possibly in doing so, insoluble aggregates within neurons are taken up and degraded by microglia as well[12-14]. This in turn, produces toxic oligomers that can spread to other parts of the brain and induce pathogenic protein aggregation in these areas[15-17]. What is more, engulfment of aggregates by microglia instigates secretion of cytokines such as IFN-γ[16-18].

Microglia in their M2 state inherently possess a neuroprotective role in the central nervous system, attenuating pro-inflammatory signalling and downregulating proliferation of T helper cells[10,17-20]. However, upon a sustained pro-inflammatory stimulus, the neuroprotective characteristics of M2 microglia switch to an inflammatory response in the M1 activated state[20-23]. This pro-inflammatory signalling fosters a chronic inflammatory environment in the brain which leads to further overactivation of surrounding microglia and the immune system,

targeting diseased but also healthy neurons and further leading to the degeneration of neuronal functions, aggravating neurodegenration. Chronic neuroinflammation is another common feature of neurodegenerative disorders, which together with neuronal degeneration are thought to drive progression of AD and PD[16,24,25]. On the cellular level, both the NF-κB and c/EBPβ pathways have been numerously reported to remain activated in neurodegenerative conditions such as AD, while suppression of these pathways have been associated with neuroprotection[26-29,30]. Understanding the mechanisms controlling neuroinflammatory responses in microglia and other glial cells may unveil additional targets implicated in neurodegenerative pathologies.

In addition to aggregate-stimulated activation of microglia, other factors have also been described to sustain chronic inflammation, including the ubiquitin-proteasome system (UPS)[4,31]. Since proteasomes play vital roles in regulating processes ranging from gene transcription and intracellular signalling to degradation of misfolded proteins, the UPS is likely to regulate inflammatory pathways on several levels[32,33].

1.2 Ubiquitin-Proteasome System

The standard 26S proteasome holoenzyme is a multicatalytic complex abundantly present in all eukaryotic cells. It is comprised of a barrel-shaped 20S proteasome core particle (CP) containing three proteases (β_5, β_2, and β_1), along with one or two 19S regulatory particles (RP) bound to either ends of the CP (**Figure 1**). Within the last decade, a potential regulatory role of the UPS involved with immune surveillance and inflammatory signalling through NF-κB activation has been identified[34,35]. A variant of standard proteasomes (sPs), known as immunoproteasomes (iPs), is upregulated under inflammatory conditions and has been suggested to hold regulatory functions during neuroinflammation[25,36]. Under inflammatory stress, the three

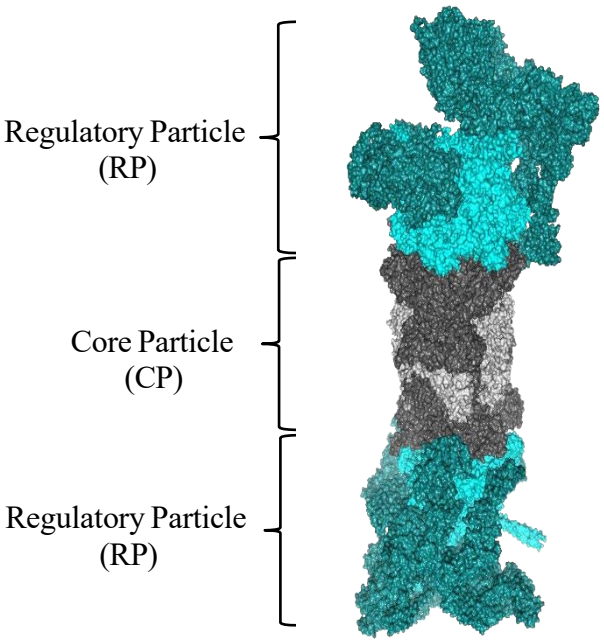

Figure 1. Standard 26S proteasome. Core particle (dark grey) containing three catalytic subunits (light grey), with one or two regulatory particles (green) bound to either side.

proteases of the sP are replaced with protease subunits of the iP, β_{5i}, β_{2i}, and β_{1i}. These immunospecific subunits substitute their corresponding sP subunits in a mutually exclusive manner (**Figure 2**). All three iP subunits are induced by pro-inflammatory cytokines, most notably TNF-α and IFN-γ[37], and together distinguish the iP from the sP. Another cytokine-activated proteasomal particle, the 11S regulatory particle (PA28α/β), may cap the CP in a similar fashion to the 19S RP, resulting in stimulation of antigenic peptide production[38-40]. Furthermore, hybrid proteasomes also exist when different combinations of iP and sP subunitsare present within the same proteasome, adding further complexity to the heterogeneity of proteasomes within an immune-activated cell[41].

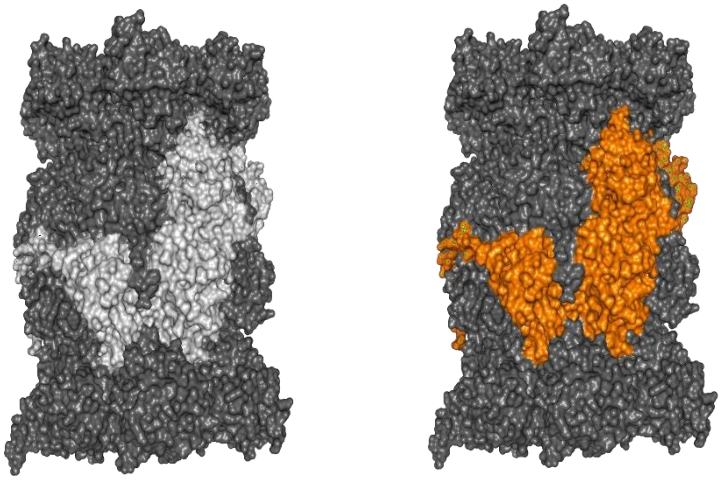

Figure 2. CP of sP versus iP. sP catalytic subunits: β_5, β_2, and β_1 (light grey) are replaced by corresponding iP catalytic subunits: β_{5i}, β_{2i}, and β_{1i} (orange).

The UPS can be regarded as a protein quality control machinery that degrades damaged or obsolete intracellular proteins[41-42]. It has been reported that the UPS degrades aggregates into more toxic oligomeric species[43], potentially being the cause of spreading and inflammation. Furthermore, when oligomers are ubiquitin-modified these may be competently degraded by the proteasomes[44].

However, other studies showed that aggregate accumulation impairs the proteasome by stabilizing it in a closed conformation and inhibiting degradation[5]. This is in line with several studies that have reported an increase in iP activity in post-mortem AD and PD brain samples, which may be in response to potentially lost sP activity due to inhibition[36,40]. The increased iP activity was further correlated to increased secretion of inflammatory cytokines such as TNF-α and IL-6[36]. On the contrary, inhibition of immunoproteasome subunits, in particular the β_{5i} subunit, suppressed inflammation and microglial activation with fewer cytokine release[45]. The continued pro-inflammatory signalling leads to an upregulation of MHC class I and II complexes, which stimulate T cells from a Th2 into a Th1 state[46-48]. Th2 cells release anti-inflammatory cytokines such as IL-4 and IL-13 to promote the neurotrophic M2 phenotype of microglia which confers neuroprotection and suppressed inflammation. On the other hand,

Th1 cells release IFN-γ which sustains the neurotoxic M1 state of microglia and further T cell recruitment[49,50]. Although the exact pathways by which the UPS regulates inflammation in neurodegenerative diseases is currently not well studied, a few studies point to the NF-κB pathway, and c/EBPβ pathways in other pathologies[51-57]. Inhibition of iP activity may therefore be a critical novel approach to targeting chronic neuroinflammation through suppression of cytokine release and could ultimately suppress neurodegeneration.

1.3 Project Aims and Hypotheses

The overarching aim of this MPhil is to study the relationship between the proteasome, specifically the immunoproteasome, and the inflammatory pathways that lead to neurodegeneration. To achieve this, I will pursue the following goals:

(1) **Understand the mechanism of proteasome foci formation in the presence of aggregates.** In this laboratory we observed proteasome foci forming in response to aggregate treatment. Previous studies have shown that proteasomes accumulate and form foci during osmotic stress in a liquid-liquid phase separated (LLPS) manner. Based on this, I hypothesize that proteasomes and immunoproteasomes form foci in an LLPS-manner to sequester and enhance degradation of aggregates. The objective here is to determine if standard or immunoproteasomes form foci around the aggregates, and the mechanism by which they form. Live-cell imaging and super-resolution microscopy will be used to visualize foci formation under different treatments.

(2) **Decipher the mechanism by which immunoproteasomes modulate microglial activation.** Although inflammation has been linked to neurodegeneration through the β_{5i} and β_{2i} subunits, the mechanism that aids or hinders the progression of this pathology remains unclear. I hypothesize that the immunoproteasome is directly responsible for regulating the NF-κB and c/EBPβ pathways in aggregate-induced inflammation. Live-cell imaging and super-resolution microscopy will be used to understand the expression and localization of proteasome subunits under different inflammatory stimuli.

It is important to understand how proteasomes target aggregates, how they sustain chronic inflammation, and its implication for cellular proteostasis. This knowledge will enlighten the mechanism of these neurodegenerative pathologies and will aid in the selection of better treatments with fewer side effects attributed to UPS impairment.

2. Methods

2.1 Cloning

To visualize the proteasomes the β_5 (sP) and β_{5i} (iP) subunits were tagged with a fluorescent protein. These subunits were chosen since they are mutually exclusive and thus cannot coexist in the same proteasome. This means that there is confidence in that an observed fluorescent signal is coming from either the standard or the immunoproteasome. This differentiation is crucial when understanding if the role of the proteasome system is dependent on species and localization. *PSMB8* which encodes human β_{5i} ($h\beta_{5i}$, Addgene #86773), or *PSMB5* which encodes human β_5 ($h\beta_5$, Addgene #86769) were fused downstream to the DNA sequences coding for eGFP, mEos4b or SNAP-tag in a pcsII vector. NEBuilder was used to clone these fusion constructs.

CRISPR-cas9 mediated genome editing was carried out with pSp-Cas9(BB)-2A-Puro (Addgene # 48139) containing the guide RNA (gRNA) of choice. To knock-in a DNA sequence downstream of the proteasomal gene, a gRNA was designed to cleave right before the stop codon. To knock-out a gene, a gRNA was designed to target the first axon that differs from other proteasomal subunits, refer to Table 1. This is because *PSMB5* and *PSMB8* are highly homologous, specially towards the beginning of the gene. To clone the specific gRNA into the Cas9 plasmid, restriction enzyme digestion and ligation protocols specified in Zhang et al were followed[58]. The HRTs (homologous repair templates) were designed to have the DNA sequence of mEos4b flanked with 500-700 bp of homology arms of the gene of interest (either *PSMB8* or *PSMB5*) on either side of the stop codon. HRTs were cloned into pUC-GW-KAN by GENEWIZ.

Table 1: gRNA for CRISPR editing

gRNA	Sense	Purpose	Target	Sequence
crKP001	5’	Knock-out	*hPSMB8*	caccgGTGCAGCAGACTGTCAGTAC
crKP001	3’	Knock-out	*hPSMB8*	aaacGTACTGACAGTCTGCACc
crKP002	5’	Knock-out	*hPSMB5*	caccgTTTGTACTGATACACCATGT
crKP002	3’	Knock-out	*hPSMB5*	aaacACATGGTGTATCAGTACAAAc
crKP003	5’	Knock-in	*hPSMB5* stop codon	caccgACCGGGAAGCCAATCAATAA
crKP003	3’	Knock-in	*hPSMB5* stop codon	aaacTTATTGATTGGCTTCCCGGTc
crKP004	5’	Knock-in	*hPSMB8* stop codon	caccgGCTGATCTACATGAGAAGTATAG
crKP004	3’	Knock-in	*hPSMB8* stop codon	aaacCTATACTTCTCATGTAGATCAGCc

All constructs were validated by restriction enzyme digest, followed by Sanger sequencing.

2.2 Cells and Culture Conditions

Established cells lines of HEK293A expressing RPN11-eGFP (a subunit of the proteasomal RP) from the genomic locus, and LN229 were used in this study. As well as iPSC-derived microglia differentiated by Daniel Clode in Professor Paul Matthews' group, according to the published protocol in Haenseler et al[59].

All cells were cultured in a humidified incubator at 37°C and 5% CO2, from now on referred to as standard conditions.

Established cell lines were grown in Dulbecco's Modified Eagle Medium (Gibco) supplemented with 10% fetal bovine serum (Gibco, South America), 2 mM L-glutamine (Gibco), and 100 U/mL penicillin-streptomycin solution (Gibco). This media composition will be referred to as D10. iPSC-derived microglia were cultured under standard conditions in medium composition optimised by the Matthews lab (manuscript in preparation).

All cell lines were tested for mycoplasma contamination using Jena Bioscience Mycoplasma Detection Kit (cat.# PP-401L). Mycoplasma contaminated cells were then cleaned with Sigma-Aldrich LookOut Mycoplasma Elimination Kit (cat.# MP0030-1KT). Cell lines were re-tested for mycoplasma after two weeks of being cleaned to ensure no contamination remained, and every 6 months thereafter. All mycoplasma testing and elimination was carried out according to the corresponding manufacturer's protocol.

2.3 Cell Line Manipulations

Cells were transiently transfected using jetOPTIMUS DNA Transfection Reagent (Polyplus-transfection) following manufacturer's protocol, in tissue culture-treated plates. The cell cultures were incubated overnight with the transfection mixture, and washed with fresh D10 the next morning, followed by a 48-hour minimum recovery period before imaging.

Osmotic stress was induced by incubating the cells with 150 mM KCl solution in D10 medium. To induce aggregate stress, cells were incubated with 1 μM αSyn, or 0.5 μM αSyn covalently labelled with AlexaFluor-647 (αSyn-647) in the specified medium for 24 hours.

Liquid-liquid phase separation was disrupted by treating with 1% 1,6-hexanediol in the medium specified for 30 minutes.

The cytoskeleton was disrupted by treating the cells for 20 minutes at 37°C with 5 μM final concentration of Latrunculin A to prevent actin polymerization, or Colcemid to target microtubules. As a vehicle control, DMSO alone was added at the same volume to control cells.

2.4 Establishing Cell Lines

To produce CRISPR-edited knock-in cell lines, plasmid pSp-Cas9(BB)-2A-Puro containing a gRNA targeting the gene of interest's stop codon was transfected, along with an HRT into 0.25 $\times 10^6$ LN229 cells. The transfected cultures were left to recover for 2 weeks before sorting with BD FACSDiva 8.0.1 (BD Biosciences), performed by Dr Bhavik Patel at the MRC-Imperial-BRC flow cytometry core. Single cells were expanded for at least four weeks before confirming corresponding fluorescence through flow cytometry using BD FACSMelody System (BD Biosciences). All FACS data was analyzed using FCS Express Flow Cytometry software version 6 (De Novo Software). To identify cells carrying the correct knock-in sequence, genomic DNA (gDNA) was purified from 1×10^6 cells per monoclonal line using Monarch genomic DNA purification kit (NEB) according to manufacturer's guidelines. The gDNA was subsequently used as template for colony polymerase chain reaction (PCR). The forward primer was designed to complement the 3'-end of the last axon of human *PSMB8*, while the reverse primer amplifies from the start of the gene's UTR. The products were ran on a 1.2% agarose gel containing SYBR Safe in TAE (Tris-acetate-EDTA) buffer by electrophoresis at 100 V. Successful insertion of the gene coding for mEos4b at the 3'-end of human *PSMB8* would yield a 955 bp amplicon, while no insertion would yield a 271 bp amplicon.

To establish a cell line with stable ectopic expression of Ub^{G76V}-Dendra2, 0.25×10^6 LN229 cells were transfected with pCMV-Ub^{G76V}-Dendra2, and after a 48-hour recovery period, cells were selected with 600 µg/mL G418. Medium containing antibiotic selection was changed every three days for two weeks. Monoclonal cell lines were then obtained by performing limiting dilution of 0.5 cell per well seeded into 96-well plates. While the cells were seeded in 96-well plates, the media containing antibiotic selection was replenished every seven days.

2.5 Native Gel Electrophoresis

Pellets from cells expressing tagged proteasome particles were mildly lysed in proteasome buffer (50 mM NaH_2PO_4 at pH 7.5, 100 mM NaCl, 10% Glycerol, 5 mM $MgCl_2$, 0.5% NP-40, 5 mM ATP, 1 mM DTT) containing a cocktail of protease and phosphatase inhibitors (Thermo Fisher Scientific, Pierce, cat.# A32961). The lysate was cleared by centrifugation at 20,000 × g for 25 minutes at 4°C. 20 µg of the cleared lysate was loaded onto a 3.5% native gel and ran in a cold room at 100 V for 3 hours, according to Roelofs et al[60]. Native gels were visualized with iBright FL1500 Imaging System (Thermo Fisher Scientific).

2.6 α-Synuclein Aggregation

Fibrils were assembled from 70 μM purified αSyn monomers in aggregation buffer (25 mM Tris-Cl, 100 mM NaCl and 0.1% NaN_3) using a DNA lo-bind microcentrifuge tube. The reaction was agitated at 200 rpm, at 37°C for 72 hrs. To visualize fibrils in a cellular setting, αSyn aggregates, αSyn monomers conjugated to AlexaFluor-647, and unmodified αSyn monomers were mixed in a 1:2:20 molar ratio and assembled into aggregates as described above. To increase efficiency of cell penetration, fibrils were sonicated at room temperature for 15 minutes as per the laboratory protocol before adding them to the culture medium, so they were not characterized.

2.7 Immunocytochemistry

Cells were washed with Ultrapure PBS prior to fixation in the presence of 4% paraformaldehyde and 0.2% gluteraldehyde at 37℃ for 30 minutes. After another washing step to remove the fixatives, cells were permeabilized with 0.1% Triton X-100 in PBS at 37°C for 30 minutes. To ensure quenching of gluteraldehyde, 0.4 M glycine in PBS was added to the cells and incubated at 37℃ for 20 minutes, followed by blocking overnight at 4°C in blocking buffer (2% glycine, 2% bovine serum albumin, 0.2% gelatin, 50 mM NH_4Cl, diluted in PBS). On the next day, the blocking buffer was removed, and the cells were then incubated overnight at 4°C with primary antibody diluted in blocking buffer to concentrations listed in Table 1. On the final day, cells were washed 3 times with PBS for 5 minutes per wash before the last blocking step was performed for 15 minutes. Secondary antibody was then added to the blocking buffer and incubated for 30 minutes at room temperature. To remove excessive secondary antibodies, 3 × blocking buffer followed by 3 × PBS washes were repeated. DAPI diluted in PBS was added at a final concentration of 1 μg/mL for 30 minutes before washing with PBS twice to facilitate identification of cell nuclei under the microscope.

Table 2: Antibodies for Immunocytochemistry

Antibody	**Dilution**	**Species**	**Vendor**	**Catalogue #**
β_5	1:100	Mouse anti-Human	Santa Cruz Biotechnology	sc-365699
β_{5i}	1:100	Rabbit anti-Human	Abcam	ab3330
Alexa Fluor 488	1:2000	Goat anti-Rabbit	Invitrogen	A11008
Alexa Fluor 488	1:2000	Rabbit anti-Mouse	Invitrogen	A11001
Alexa Fluor 568	1:2000	Goat anti-Mouse	Invitrogen	A11004
Alexa Fluor 647	1:2000	Chicken anti-Rabbit	Invitrogen	A21443

2.8 RNA Extraction

RNA from iPSC-derived microglia at 24 and 72 hours post inflammatory stress was extracted using Nucleospin RNA Plus kit (Macherey-Nagel) following manufacturer's guidelines. The RNA was then stored at -80°C for later use.

2.9 Microscopy

Imaging experiments were performed on a custom-built total internal-reflection fluorescence (TIRF) microscope (Ti2 Eclipse, Nikon), mainly under the highly inclined and laminated optical sheet (HiLo) modality. Samples were prepared on 0.13 mm-thick borosilicate glass circle coverslips (VWR) in Leibovitz's L-15 medium and mounted on a metal cell chamber holder (Attofluor, Thermo Fisher). Each coverslip was plasma cleaned with argon gas for 30 minutes before cells were seeded. Fluorescence excitation was achieved using a four-color laser combiner system (C-Flex, Cobolt) with peak excitations at 405 nm, 488 nm, 561 nm and 640 nm. A typical output of 10 mW was used at the objective for routine imaging. Super-resolution fPLAM imaging and single-particle tracking were performed with typical output of 100 mW at the objective to study live cell events[5,31,32]. Fluorescence emissions were detected using the same objective (CFI Plan Apochromat Lambda D series, Nikon) (30× or 150× magnification depending on application) and recorded by a Prime95B sCMOS camera. All imaging at 150× magnification was carried out using the CFI Apochromat TIRF 100× oil immersion objective. An Optosplit (Cairn) was introduced in the emission pathway to separate fluorescence emission and enable imaging of two channels simultaneously. To achieve photoconversion of Dendra2 and mEos4b-tagged proteins, cells were excited with a 405 nm laser for two seconds at 50 mW, and subsequently visualized using the 561 nm laser (40 mW) at 150× magnification. All captured images were processed and analyzed using Fiji software and its incorporated plugins and macros (ImageJ, National Institutes of Health)[61].

3. Understanding Proteasome Foci Formation

It has been established in the literature that intracellular membraneless compartments of biomolecular condensates exhibiting liquid-like properties exist phase separated from the cytoplasm[62-64]. These biomolecular condensates are known to be involved in a wide range of functions, such as regulation in transcription, immune responses, and neuronal synaptic signaling. More recently, research suggests that one of the tasks of the condensates is to form proteolytic centers, which are foci with a higher concentration of recruited proteasomes for targeted degradation[62,64]. It has been shown that most of these condensates form through liquid-liquid phase separation, however, the details on its formation remain elusive[63,64].

3.1 Results and Discussion

3.1.1 Aggregate-Stress Induced Foci are not Liquid-Liquid Phase Separated

To study how proteasomes are recruited and accumulated around aggregates, HEK293A cells expressing RPN11-eGFP were used in this study. HEK293A RPN11-eGFP cells were first transfected with a plasmid encoding for nuclear lamina marker Lamin B1 fused with mCherry (**Figure 3**, red). Aggregates from recombinant αSyn monomers were added to the transfected HEK293A cells the day after the transfection. After 24 hours of αSyn aggregate treatment, proteasome foci could be observed around the aggregates (**Figure 3A**, right). In comparison, the proteasomes of untreated cells remained dispersed throughout the cell interior, with a higher concentration inside the nucleus (**Figure 3A**, left). The formation of proteasome foci has been reported before under specific conditions such as osmotic stress, I therefore compared this foci response to aggregate-induced foci. After 5 minutes of incubation in potassium chloride (KCl), the cells showed many distinct foci in and outside of the nucleus (**Figure 3A**, middle**)**. Furthermore, the formation of high salt induced foci was recently shown to be LLPS entities that could be disrupted with 1,6-hexanediol treatment[62]. To understand whether aggregate-induced foci were also assembled through LLPS the same experiment was repeated, imaging cells under osmotic stress or treated with αSyn aggregates labelled with AlexaFluor-647 (αSyn-647). Treatment with 1% 1,6-hexanediol reversed proteasome foci that were induced by KCl within 30 minutes (**Figure 3B**). This is in contrast with the observations in **Figure 3C**, which show αSyn-647 induced proteasome foci still in cells that were treated with 1% 1,6- hexanediol. **Figure 3D** shows distinct proteasome foci co-localizing with αSyn-647 aggregates. **Figure 3C-D** were taken as a z-stack under HILO imaging, so the foci might be in a different plane than the aggregates, but the black arrows show positions of foci throughout the entire z-stack.

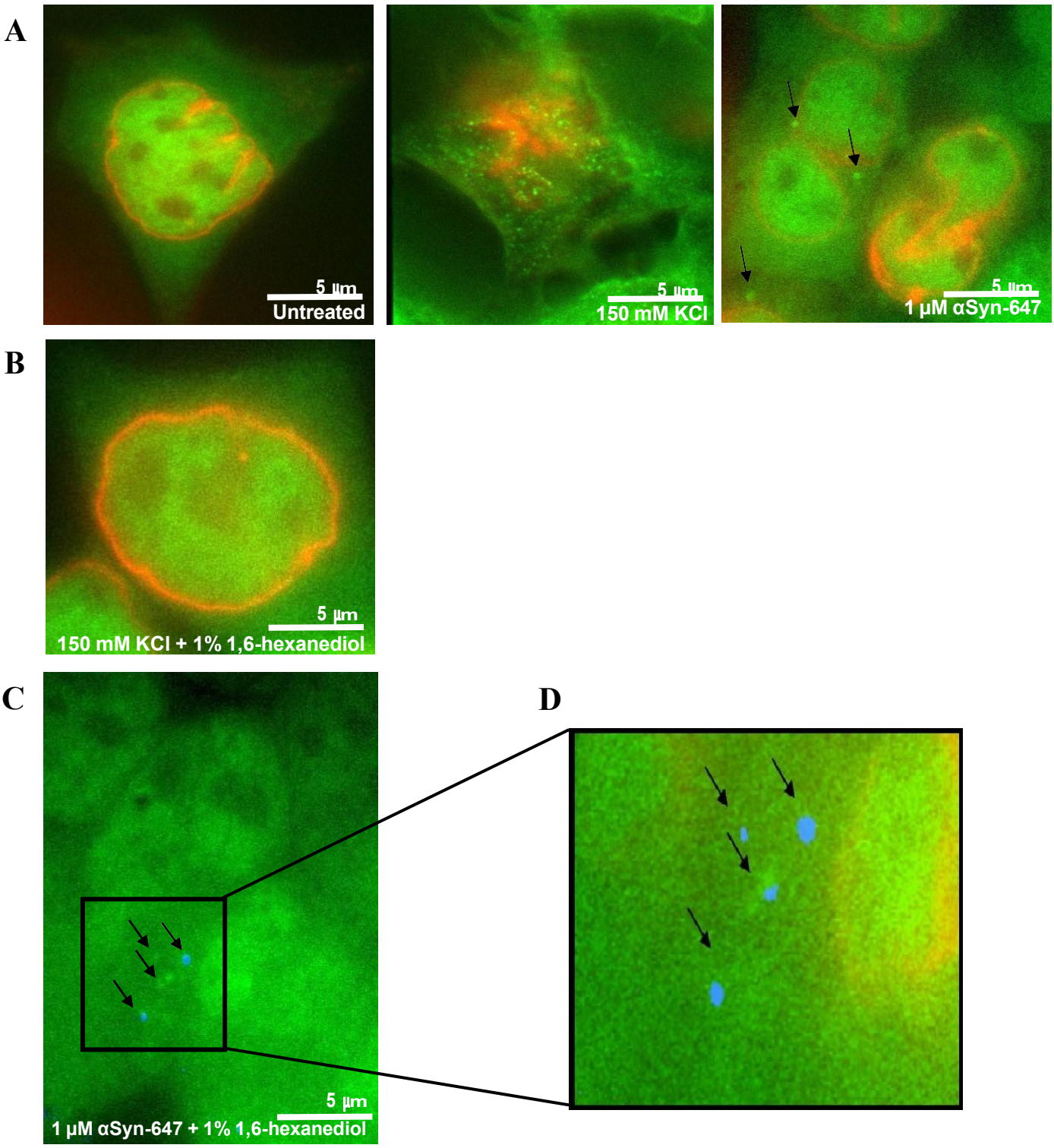

Figure 3. Aggregate-induced foci are not liquid-liquid phase separated. Proteasomes marked at RPN11 with eGFP are shown in green, and Lamin B1 marker is shown in red. **A** Osmotic stress (middle) and aggregate (right) stress-induced foci in comparison to no foci in untreated cells (left). **B** 1% 1,6-hexanediol dissolved foci in osmotic stressed cells within 30 minutes. **C** 1% 1,6-hexanediol did not dissolve foci (black arrows) induced by aggregates (blue). **D** Inset of **C**.

3.1.2 Cytoskeleton Aids in Aggregate Stress-Induced Foci Formation

The mechanism of proteasome foci assembly was further delved into to understand the process of proteasome-aggregate interactions. Proteasomes appear in a dispersed state throughout the cell without any foci formation under resting conditions, while they appear in dense foci under stress (aggregate or osmotic stress). Unpublished data acquired by other members of the lab shows no foci assembly in the presence of aggregates if the cells are pre-treated with Latrunculin A or Colcemid, which depolymerize the actin filaments or microtubules respectively. As this data is not published and I did not acquire it, it is not shown in this thesis. To complement this data, foci assembly in cells under osmotic stress induced with KCl was investigated and found that their assembly was not dependent on the cytoskeleton. Cells were pre-treated with either Latrunculin A (**Figure 4A**) or Colcemid (**Figure 4B**), and still observed foci formation after osmotic stress.

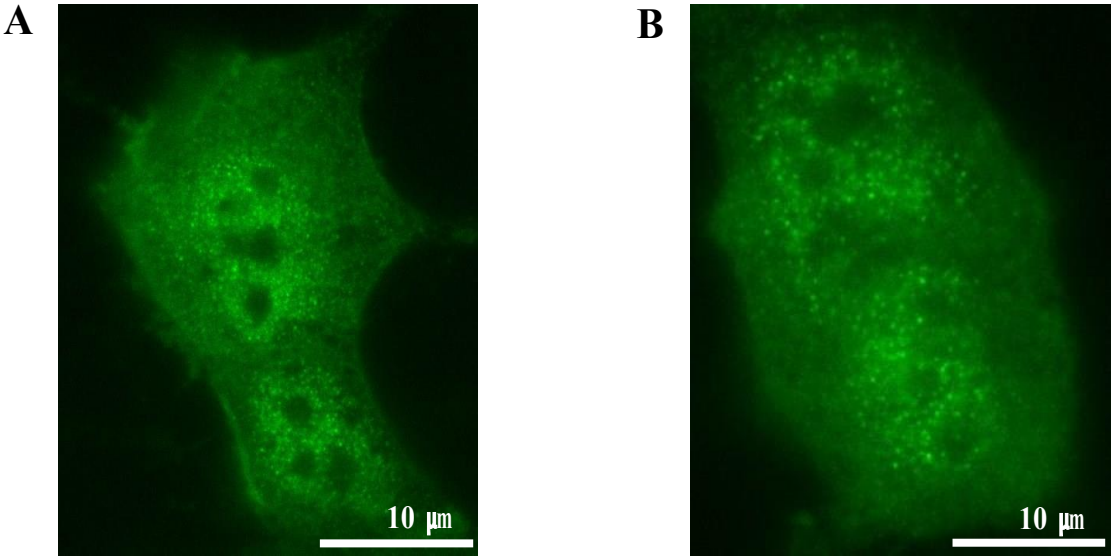

Figure 4. Osmotic stress-induced foci are not cytoskeleton dependent. Osmotically stressed cells after **A** Latrunculin A and **B** Colcemid treatment.

3.2 Conclusion

Unlike osmotic stress-induced foci, those induced by αSyn aggregates cannot be disrupted by 1,6-hexanediol, meaning that the accumulation of proteasomes due to aggregates is likely not LLPS induced. To support this observation, cells under osmotic stress could still form foci when pre-treated with a cytoskeleton disruptor. On the other hand, cells pre-treated with a cytoskeleton disruptor and stressed by aggregates did not form any foci. This data suggests that the mechanism between osmotic stress and aggregate stress foci formation is different, and that the mechanism of aggregate induced foci is cytoskeleton-dependent. The number of foci were not quantified for this experiment, however the conclusion was based on the observation that

there were either proteasome foci present or not after treatment with cytoskeleton disruptors. This work is being written up for publication combining my data with unpublished data collected from other members of the lab to provide a mechanistic basis for how proteasomes respond to aggregates in cells.

4. Deciphering the Mechanism by which Immunoproteasomes Modulate Microglia Activation

4.1 Results and Discussion

4.1.1 Fluorescently Tagged Proteasome Subunits Incorporate into the Endogenous Proteasome Complex

To endogenously tag the proteasome at the genomic level with a fluorescent protein, it first needs to be tested which of the proteolytic subunits of the sP and iP may be tagged without disrupting the integrity of the proteasome complex, enabling the distinction between sP and iP complex within the cells. Subunits β_5 and β_{5i} were selected for genetic engineering, they are encoded by the *PSMB5* and the *PSMB8* gene respectively. To test for their incorporation into their respective proteasomes, fluorescent proteins mEos4b or SNAPf were subcloned into pcsII-hβ_5 vector. To tag the immunoproteasome, fluorescent proteins mEos4b or eGFP were subcloned into pcsII-hβ_{5i} vector. In total, four fusion pcsII constructs were generated, a

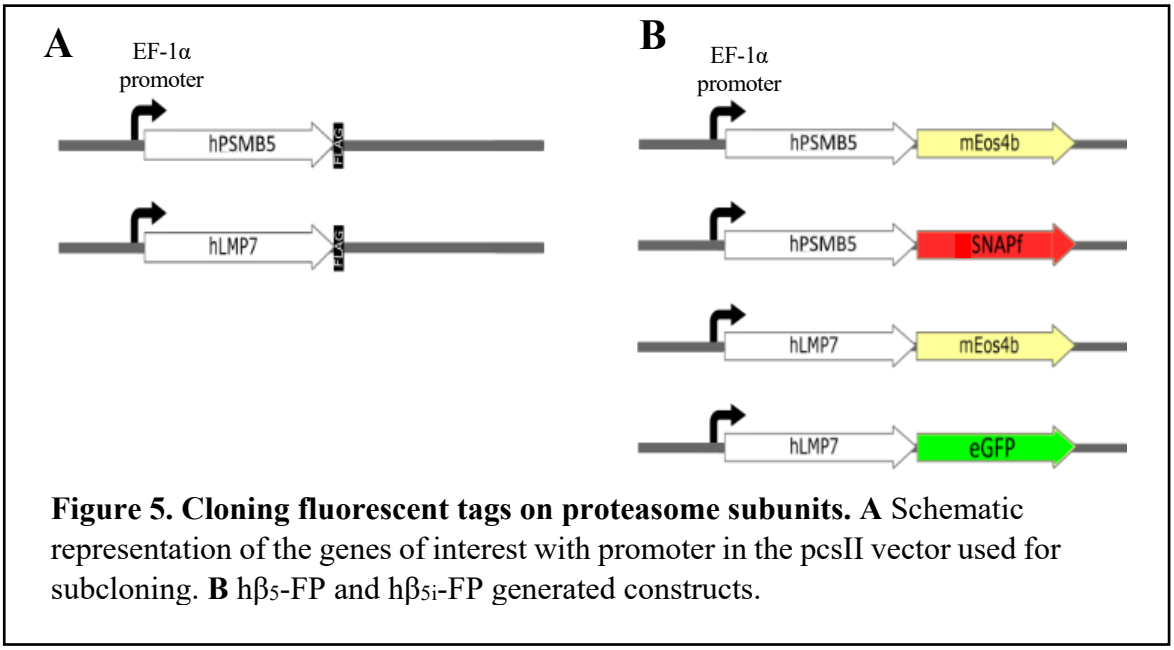

Figure 5. Cloning fluorescent tags on proteasome subunits. A Schematic representation of the genes of interest with promoter in the pcsII vector used for subcloning. **B** hβ_5-FP and hβ_{5i}-FP generated constructs.

schematic representation of the vector and fusion constructs are shown in **Figure 5A-B**, while the vector maps are shown in **Appendix figure A1-2**. The plasmids encoding for the fluorescently tagged proteasome subunits were transfected into LN229 and validated to successfully incorporate into the endogenous proteasome complex by resolving them on a 3.5% native gel electrophoresis.

4.1.2 Knocking-in FPs in LN229

Following the verification via native gel, the next step was to establish a stable LN229 culture with fluorescently tagged proteasomes as a convenient glial model of inflammation. These cells will be used to establish protocols which will be subsequently applied to iPSC-derived microglia cultures. Two gRNAs in pSp-Cas9(BB)-2A-Puro were designed to knock in mEos4b into the 3'-end of *PSMB5* gene (coding for β_5) or *PSMB8* gene (coding for β_{5i}) in LN229 via CRISPR-Cas9. **Figure 6A** shows a schematic representation of the gRNA driven by a U6 promoter, while the Cas9 gene is expressed by a β-actin promoter and flanked by two nuclear localization signals (NLS). See **Appendix Figure A3** for the vector map containing the Cas9 construct that was designed to introduce a double-stranded break before the stop codon of the gene of interest. Along with the Cas9 construct, a homologous repair template was also introduced. The repair template consists of mEos4b flanked by ~700 base pairs homology arms, excluding the gene of interest's stop codon as depicted in **Figure 6B** in red.

After two week of transfecting LN229 cells, they were confirmed to be positive for mEos4b through flow cytometry based on their green fluorescence (**Figure 6C**). The mEos4b knock-in β_{5i} line has 0.8% knockin-in efficiency, while the β_5 line was not successful at all. To obtain a monoclonal line from the mEos4b knock-in fused to β_{5i}, single cells positive for green fluorescence were sorted. Low efficiency can be explained by the fact that the homology repair template is in the bacterial pUC-GW vector, which is not optimized for replication in mammalian cells.

After four weeks of expanding the green monoclonal colonies, they were genotyped to analyse if mEos4b had incorporated at the correct site and not randomly in the genome, shown in **Figure 7**. Since there was outgrowth in 56 colonies, a PCR was first attempted by using 0.5 - 5 µL of the culture supernatant to make genotyping easier, however this PCR approach failed to produce reproducible results. The results included in this thesis are from the top 7 colonies with the healthiest morphology and outgrowth, so not all colonies are shown. From these results it can be noted that all gDNA, even that from the parental colony, produce and unexpected ban around 800 bp. In addition, all colonies yield an amplicon ~300 bp (expected 271 bp for

untagged locus), meaning that all the colonies have at least one copy of *PSMB8* that is not fused with mEos4b at the genomic level. Colonies #11 (Figure **7C**) and #55 (Figure **7A/B**) also

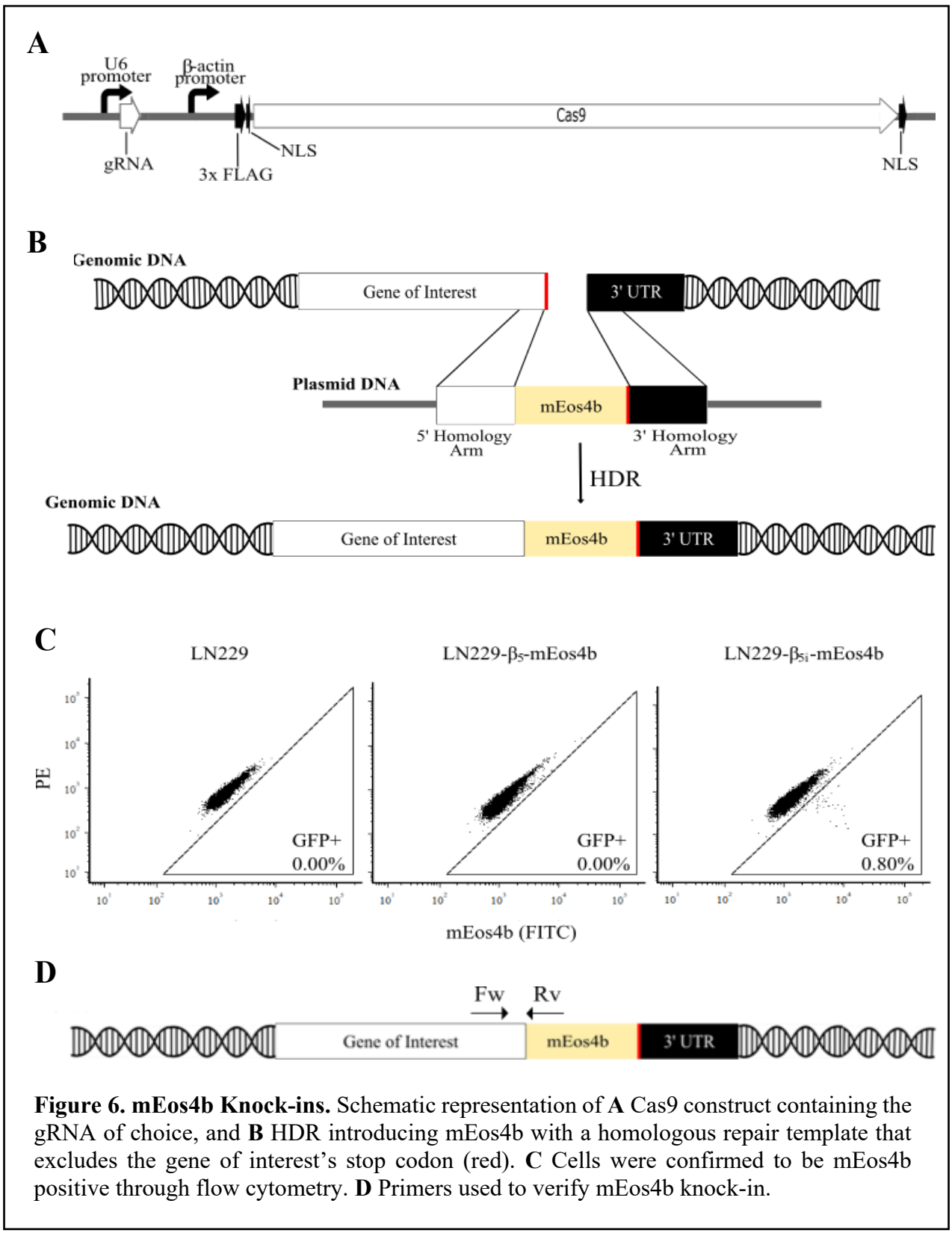

Figure 6. mEos4b Knock-ins. Schematic representation of **A** Cas9 construct containing the gRNA of choice, and **B** HDR introducing mEos4b with a homologous repair template that excludes the gene of interest's stop codon (red). **C** Cells were confirmed to be mEos4b positive through flow cytometry. **D** Primers used to verify mEos4b knock-in.

contain an additional band ~1000 bp (expected 955 bp for tagged locus), meaning that they each have one tagged and one untagged *PSMB8* locus, yielding heterozygous colonies. The

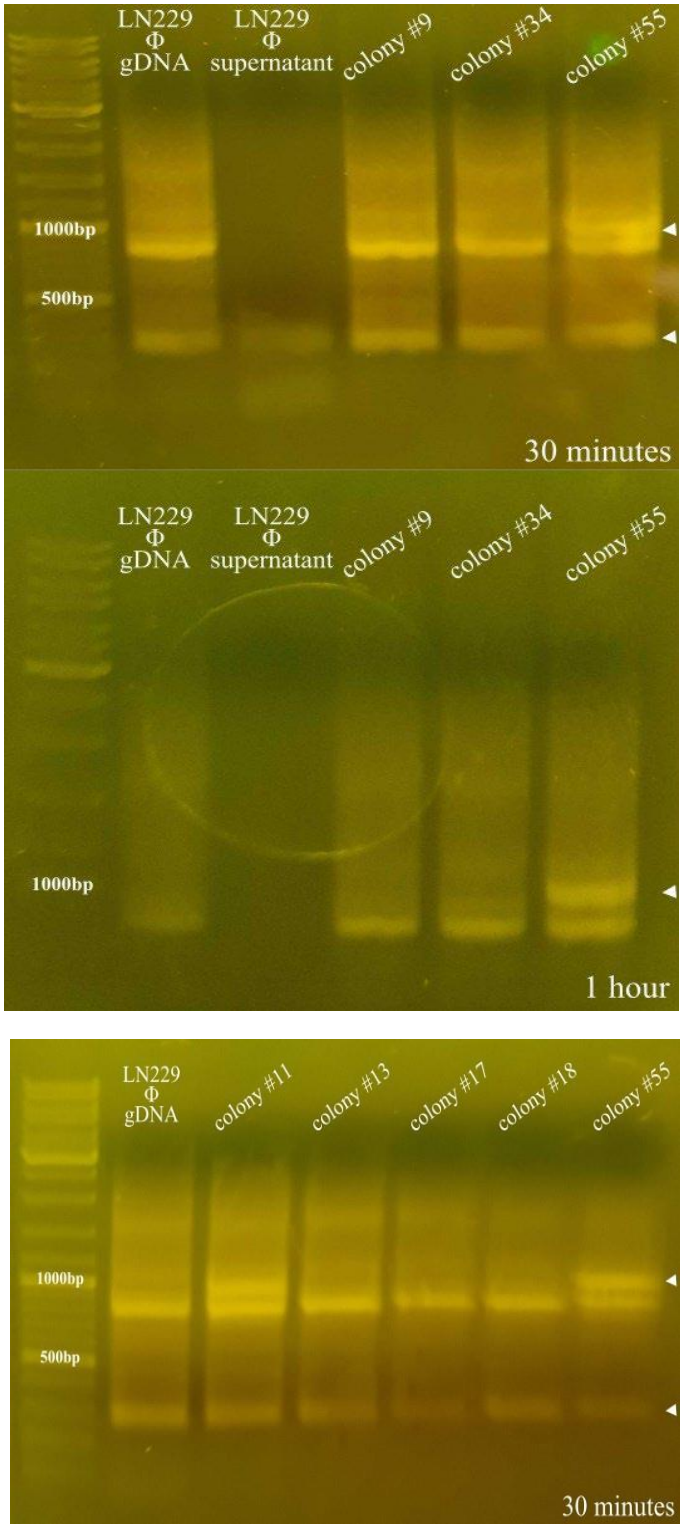

Figure 7. Colony #11 and #55 have mEos4b inserted at the correct location. DNA gel of PCR genotyping mEos4b knock-in colonies were ran at 100 V for **A** 30 minutes up to **B** 1 hour. The negative controls are on lane 1 and lane 2, from parental (wild-type) LN229. Lanes 3-5 are from gDNA of corresponding knock-in colonies. Image **C** is another batch of genotyping.

knock-in will have to be repeated to yield homozygous colonies, and re-confirmed by PCR. The PCR bands will then be extracted, purified, and sent for Sanger sequencing using a primer complementary to the DNA sequence of mEos to confirm.

4.1.3 Knock-out of Endogenous hβ$_5$ or hβ$_{5i}$ in LN229

CRISPR-Cas9 knock-outs of the β$_5$ or β$_{5i}$ subunits in LN229 were attempted, with the gRNA targeting the 5'-end of the gene. Unfortunately, all cells died. The cause of cell death is inconclusive, it could be due to the knock-out phenotype being lethal, or perhaps cell death can be attributed to a mycoplasma contamination that was present from other cell lines in the labs. If the knockouts of these proteasome genes are not viable, perhaps they can be downregulated with siRNA to study their importance on the inflammatory environment.

4.1.4 Proteasome Expression Levels Increase under Inflammatory Stress

Ultimately, the goal is to generate data from iPSC-derived microglia obtained from human patients with synucleinopathies or tauopathies. Meanwhile, I obtained iPSC-derived microglia from Daniel Clode and incubated these with either TNF-α, IFN-γ, or LPS for 24 hours (**Figure 8**) or 72 hours (**Figure 9**). The cells were then fixed and immunostained for β$_5$ and β$_{5i}$ subunits to determine their relative localization and difference in expression. During the first 24 hours, TNF-α seemed to induce β$_5$ levels (green) in the nucleus (blue), β$_{5i}$ (green) also increased in a cellular structure surrounding the nucleus, perhaps the endoplasmic reticulum or Golgi apparatus. At 72 hours, all inflammatory conditions exhibited upregulation of β$_5$ levels (pink) and β$_{5i}$ (red). At this timepoint, both subunits seemed to have significantly higher expression levels in the cell body and processes of microglia. To further investigate the inflammatory pathways involved during different inflammatory and aggregate stresses, the RNA of iPSC-derived microglia was harvested at 24 and 74 hours after treatment. Unfortunately, the RNA yield was too low to continue.

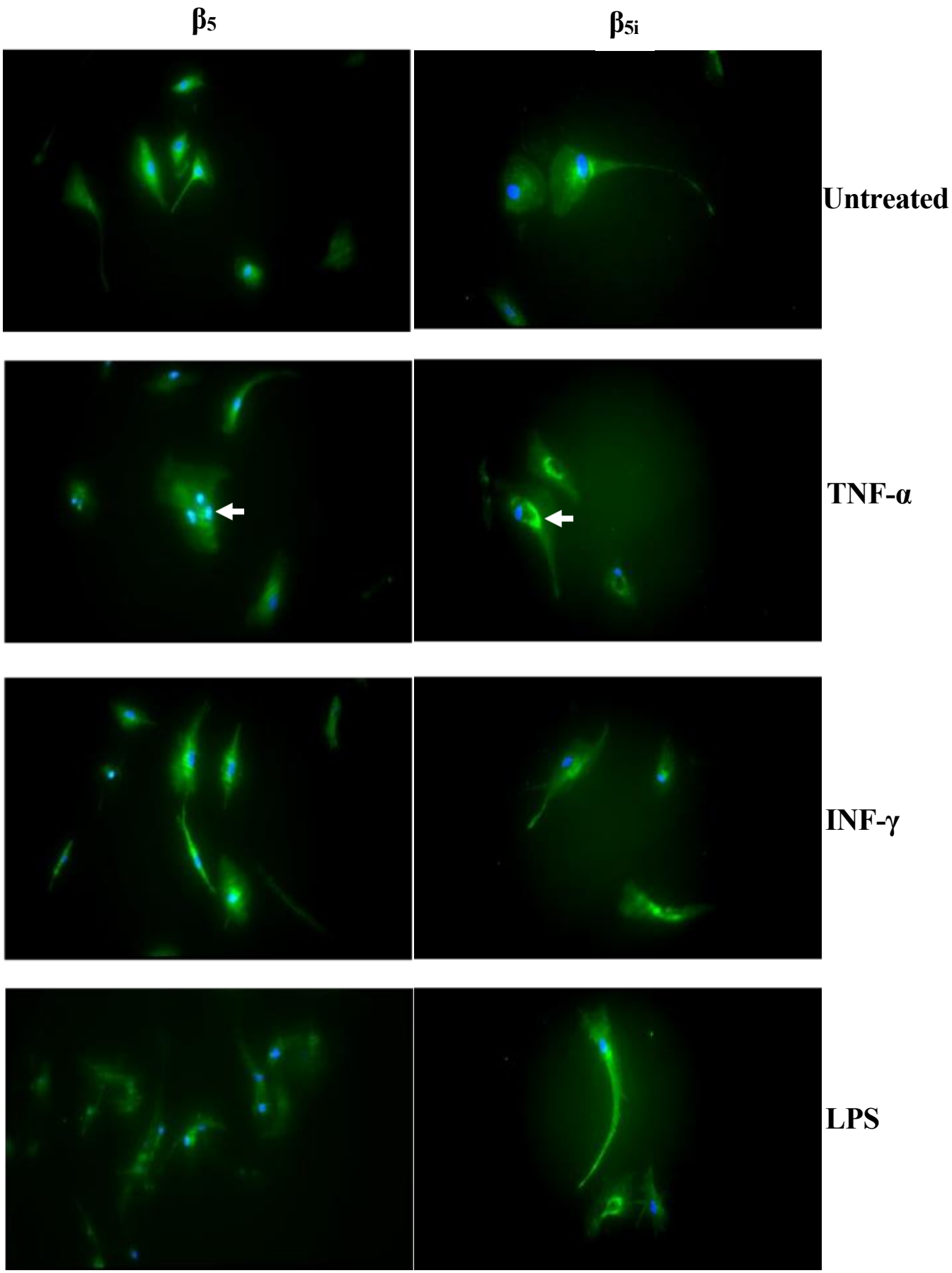

Figure 8. Inflammatory stress for 24 hours upregulates β_5 and β_{5i} subunits. Immunostaining shows the nucleus (blue), along with white arrows which indicate a clear upregulation of the proteasome subunit (green).

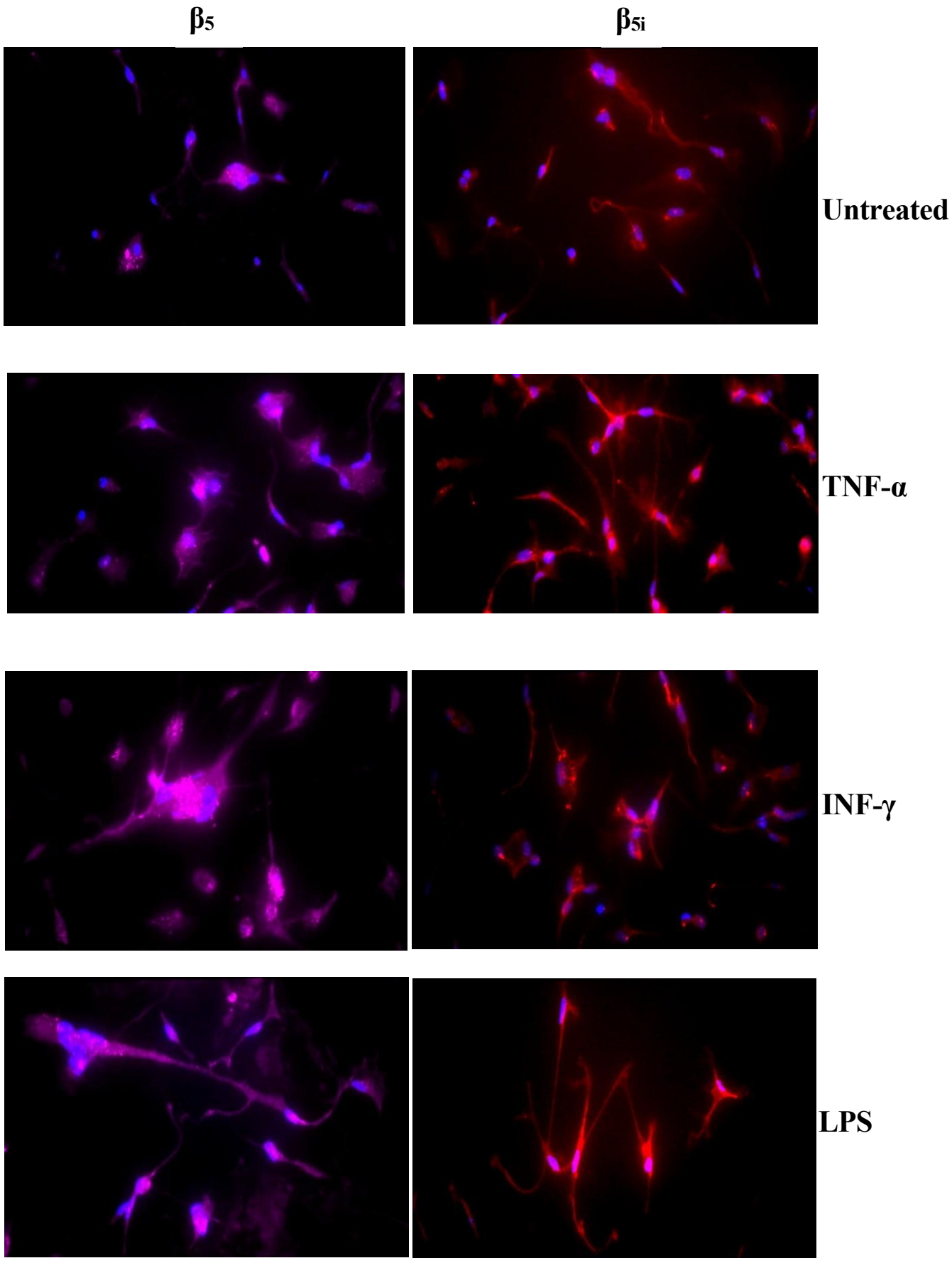

Figure 9. Inflammatory stress for 72 hours upregulates β_5 and β_{5i} subunits. Immunostaining shows the nucleus (blue), β_5 (pink), and β_{5i} (red).

4.1.5 Establishing a Proteasome Degradation Assay: Ub^{G76V}-Dendra2

To study how different conditions, such as different aggregate species, interfere with proteasome activity, I established a proteasome degradation reporter system in LN229 cells. This reporter consists of a ubiquitin moiety fused to the N-terminus of Dendra2, a photoconvertible fluorophore. The ubiquitin carries a mutation, G76V, to prevent its deubiquitination. The functional ability of Dendra2 is that it can be photoconverted by a 405 nm laser from a green fluorescent protein to a red, in a non-reversible manner (**Figure 10**).

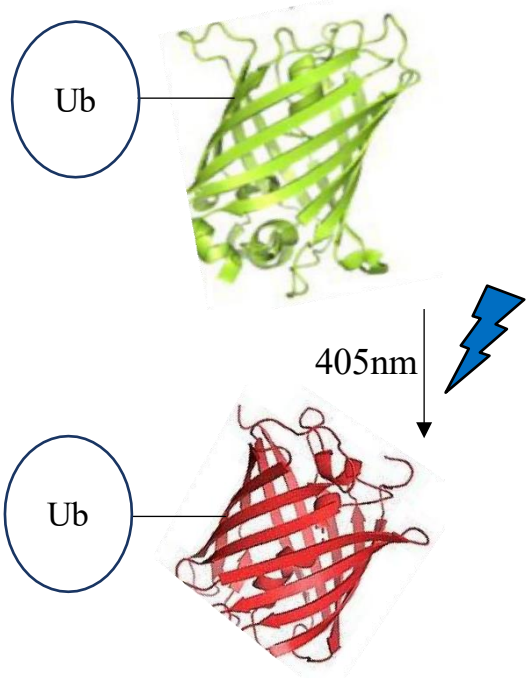

Figure 10. **Schematic representation of Ub^{G76V}-Dendra2.** Dendra2 photoconverts from green to red after a 405 nm laser stimulation.

Photoconverting allows degradation of Dendra2 to be measured in the red channel independently of synthesis of novel reporter proteins[65,66]. pCMV-Ub^{G76V}-Dendra2 construct was transfected, and then selected against G418 for two weeks. After selection, several monoclonal lines were obtained and evaluated against each other.

64 potential monoclonal lines were checked for photoconversion ability using a microscope, a representative cell line is illustrated in **Figure 11A**. The six best photoconvertible Ub^{G76V}-Dendra2 positive colonies were further verified via flow cytometry (**Figure 11B**) for green fluorescence (FITC, green histogram) and red fluorescence (PE, red histogram) before photoconversion compared to wild-type LN229 (grey). **Figure 11B** shows that colony #5 fluoresces in the red channel prior to photoconversion, and colony #7 appears to be composed of two populations, thus both colonies were discarded from the selection pool. It is necessary to understand the limitations of the Ub^{G76V}-Dendra2 degradation system. For instance, previous studies have found that degradation rate differs amongst cell types[66]. Therefore, my established system will reflect degradation of astrocytes, immune cells that readily assemble immunoproteasomes under inflammatory stress.

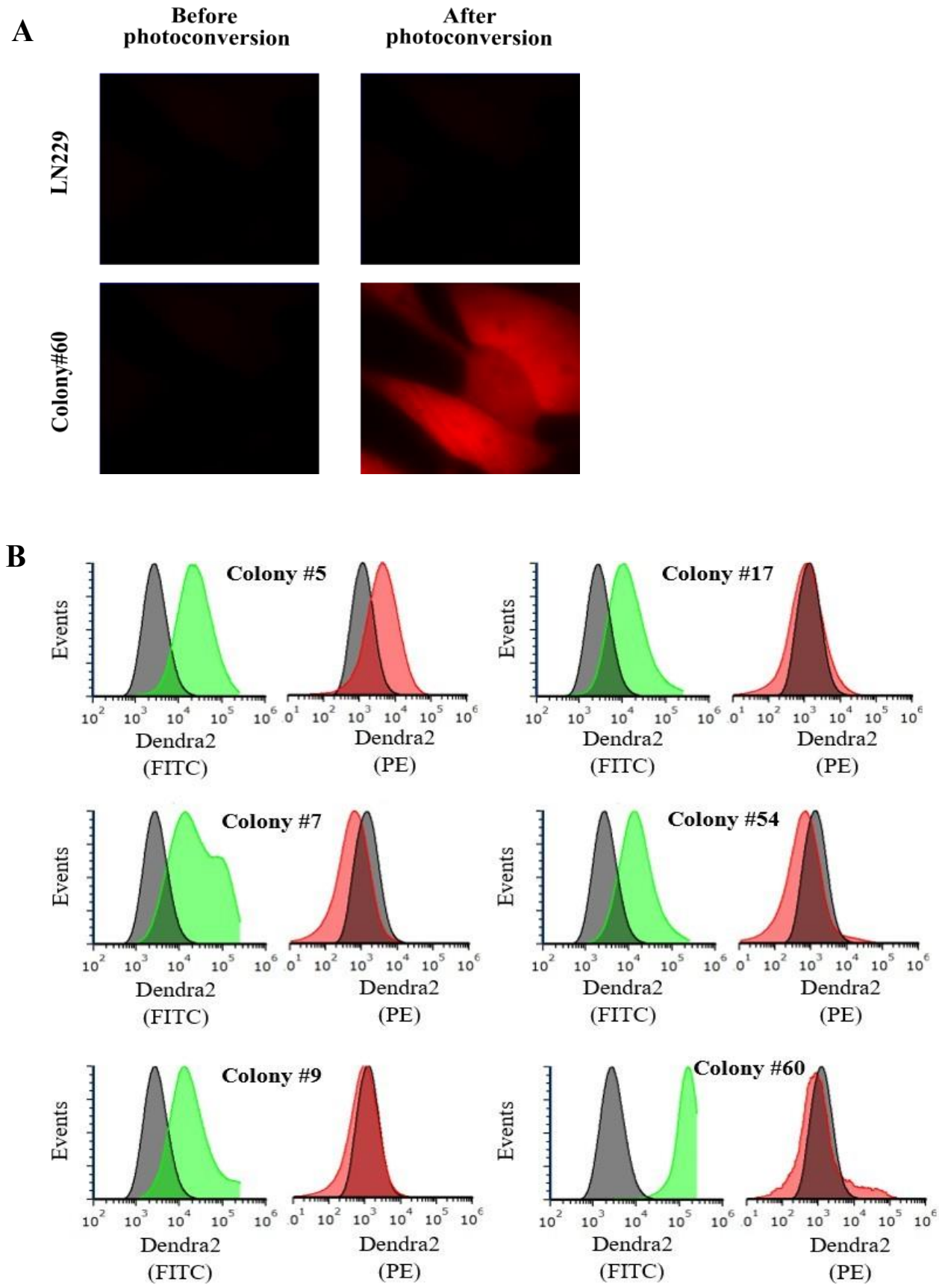

Figure 11. Selecting LN229-Ub^{G76V}-Dendra2 clones. A Photoconversion of colony #60 with 405 nm laser. **B** Flow cytometry analysis of Dendra2 FITC (green) and PE (red) fluorescence compared to wild-type LN229 cells (grey) before photoconversion.

4.2 Future Studies

Although CRISPR mediated knock-in seemed to have worked when targeting β_{5i}, it did not incorporate at the 3'-end of β_5. This is surprising as the β_5 and β_{5i} share 77% sequence identity and are close to being structurally identical. Since I used a bacterial vector for the homology repair template in a mammalian cell line it will not have replicated, thus relying on small copy numbers. To improve mEos4b incorporation at the β_5 locus, the homology repair template can be expressed on a mammalian vector for higher expression levels, and thus a higher chance of incorporating into the genome. The CRISPR knock-out culture was unsuccessful since all the cells died. There is a review on the proteasome system stating that knock-out of sP subunits will result in a lethal phenotype, while knock-out of iP subunits are viable[67]. To improve survival and selection, a homology repair template which ablates proteasome subunit function while conferring antibiotic selection such as Puromycin can be introduced. Before re-transfecting with CRISPR plasmids, LN229 cells must be confirmed to be mycoplasma negative. If this is again not viable, other proteasome subunits can be targeted. As a contingency plan, other methods can be approached, such as downregulating expression of these subunits with small hairpin RNA[68]. These knock-outs of β_5 or β_{5i} subunits in the iPSC cultures will help understand the role of the proteasomes during inflammation and aggregate spreading.

To further look at the sP and iP in microglia, I obtained preliminary data from iPSC-derived microglia that show an upregulation of both β_5 and β_{5i} under inflammatory stress. However, 30× magnification cannot resolve in enough detail the proteasome to pinpoint which cellular structure is located in. TIRF microscopy at 150× magnification can be performed to visualize the precise position of these subunits within cells. To better understand their localization, cells should be co-stained for markers of the plasma membrane, endoplasmic reticulum, and Golgi apparatus. As the RNA yield obtained from the iPSC-derived microglia was too low to proceed with the experiments with the number of RT-qPCR targets shown in **Figure 12**, first the laboratory must set up its own iPSC culture. The next couple of months the laboratory will be dedicated to establishing an iPSC-derived microglia culture from human patients harbouring tauopathies or synucleinopathies. These cultures will be the underpinning disease model of all future studies. Already in the lab, there are iPSC lines with a mutant *MAPT* (gene encoding for tau), and its isogenic wild-type correction from a frontotemporal dementia patient, as well as a *SNCA* (gene encoding for αSyn) and the isogenic duplication line from a PD patient. The purpose of the iPSC-derived microglia from human patients is to obtain data that is more relevant to a pathology, rather than in immortalized cancer cell lines. After

establishing these microglia cultures, fluorescent proteins can then be fused to the proteasome subunits just as it was already attempted in the LN229 cells. These cells will allow for the understanding between the interactions of the proteasome complex with aggregates, as well as the interplay between the standard and immunoproteasome in the presence of aggregates and inflammatory stress.

Proteasome subunits	NFκB pathway	Oxidative stress	Cytokines	Associated genes	Microglial markers	Reference genes
β_2	NEMO	COX2	CCL3	CASP1	P2YR12	GAPDH
β_5	NFκB1	HIF1α	CCL4	c/EBPβ	TMEM119	HPRT1
β_{5i}	NFκB2	NLRP3	FOXP3	HLA-DRA		RPL13
β_{2i}	NFκBIA	NOS1	IL1-α	NOD2		
β_{1i}	NFκBIζ	NOS2	IL1-β	Per2		
PA28α	NIK	NOS3	IL-6	TLR4		
PA28β	MyD88	Nrf1	IL-8	TREM2		
Rpt3	RelA	Nrf2	IL-10			
Rpt5	TNF-α		IL-12			
			IL-16			
			IL-17A			
			IL-23			
			TGF-β1			
			TNF-α			

Figure 12. qPCR targets of inflammation.

5. Future Work

One of the objectives of this thesis was to delve into how proteasomes form foci in the presence of αSyn aggregates. As shown in **Figure 3**, cells that were incubated with αSyn aggregates for 24 hours formed distinct proteasome foci co-localizing to the aggregates. Recent studies have shown that cells under osmotic stress also form proteasome foci which are liquid-liquid phase separated[68], shown by dissolving the condensates with 1% 1,6-hexanediol, an LLPS disruptor. However, proteasome foci observed in response to αSyn aggregates were not able to be dissolved in 1% 1,6-hexanediol, suggesting that these foci are formed through a different mechanism to LLPS. Unpublished data collected by other members of the lab shows that foci formed in response to αSyn aggregate stress can be inhibited if the cells are treated with cytoskeletal disruptors, Latrunculin A and Colcemid. In contrast, foci formed due to osmotic stress cannot be inhibited when treated with cytoskeletal disruptors. This evidence is highly indicative that unlike the LLPS-induced foci formed under osmotic stress, foci formed in response to αSyn aggregates are assembled via the cytoskeleton. To better understand the differences between osmotic and aggregate stress-induced foci, these two different entities must be super-resolved.

A limitation of this work is that all experiments attempting to understand foci formation, even in the literature, focuses on understanding the sP and not the iP. To obtain some insight into how the immunoproteasome responds to αSyn aggregates, the experiments should be repeated on cells with fluorescently tagged iP. Ideally, in iPSC-derived microglia harbouring a synucleinopathy. I hypothesize that these lines will naturally have sP and iP foci throughout the cell body co-localizing with the aggregates formed due to their mutation. However, if not, these cells can also be stressed with exogenous recombinant aggregates to attempt to induce foci formation and observe integrity with LLPS as well as cytoskeletal disruptors. This work will allow for a further understanding into the role and interactions of the immunoproteasome against αSyn aggregates, and the mechanism behind foci formation in cells.

The second objective of this thesis attempted to understand the mechanism by which immunoproteasomes modulate microglial activation. One aspect to study was the localization and mechanism of the sP and iP in response to stress, so cell lines with fluorescently labelled β_5 and β_{5i} had to be set up first. A CRISPR/Cas9 system targeting the 3' end of β_5 and β_{5i} was transfected into LN229, along with an HRT coding for mEos4b. As shown in **Figure 6C**, the HRT mEos4b knock-in β_{5i} line had 0.8% knockin-in efficiency, while the β_5 line did not successfully incorporate the HRT at all. To obtain monoclonal LN229 which stably expresses

mEos4b, the transfected pool was sorted for green fluorescent cells, and as shown in **Figure 7** eventually genotyped to conclude if mEos4b had been incorporated at the correct site in the genome. Only two monoclonal lines, #11 and #55, produced a band that suggest the insertion of mEos4b at the correct locus, however, they also produced a band suggesting an untagged locus. From this data, it can be concluded that both lines are heterozygous for mEos4b inserted at the 3' end of β_{5i} locus. Low efficiency can be explained by the fact that the HRT is cloned in pUC-GW, a bacterial vector which is not optimized for replication in mammalian cells. Both CRISPR knock-ins must be repeated, preferably with the HRT in a mammalian vector such as pcDNA3.1.

Meanwhile the knock-in cell lines were being established, iPSC-derived microglia was treated with different inflammatory stressors: IFN-γ, TNF-α, and LPS and stained with antibodies, to visualize how the sP and iP changed position and expression levels over time. Within 24 hours (**Figure 8)** TNF-α seemed to increase β_5 levels in the nucleus and β_{5i} levels in a cellular structure surrounding the nucleus, but not the other inflammatory stressors. Within 72 hours (**Figure 9**), all inflammatory conditions exhibited upregulation of β_5 and β_{5i} levels, where both subunits had significantly higher expression levels in the cell body and processes of microglia. These iPSCs had to be cultured in 96-well plates due to their low quantities and could only be imaged under 30× magnification, so apart from general localization and expression levels not much information could be extracted from these preliminary results. Before repeating this experiment the laboratory must set up its own iPSC-derived microglia culture directly on coverslips, so they can be imaged at higher magnifications. When repeating this experiment, α-Syn aggregates should also be used to understand the sP's and iP's response to this stress. Ideally, the localization will be studied through super-resolution imaging and translocation using live-cell imaging of the sP and iP under different stresses such as aggregates, but also inflammatory stresses using cytokines.

Another aspect to study was the function of the sP and iP, so I attempted to knock-out either the genes encoding for β_5 or β_{5i} in LN229. Surprisingly, neither of these cultures were viable, suggesting that these knockouts are lethal. A way to circumvent this issue is to use siRNA to downregulate β_5 or β_{5i} expression levels, or knocking-out other genes of the sP or iP complex that would halt its function yet perhaps still be viable. iPSC-derived microglia with either the β_5 or β_{5i} downregulated or knocked out, would be useful to understand the transcription profile by performing qPCR (refer to targets in **Figrue 12**) to get some guidance on the pathways involved. Importantly, this set of experiments can determine if NF-κB or c/EBPβ pathways are regulated by the iP. This data should be supported by RNA-seq to understand the

mechanisms regulated by either the sP or iP, as well as the downstream targets for each. When performing these experiments, differences amongst cells treated with aggregates, cytokines, sP or iP activators or inhibitors should be considered. Based on qPCR data showing NF-κB or c/EBPβ involvement, a dual luciferase assay in microglia can be set up to concurrently assess how different stresses activate each pathway. If RNA-seq data identifies novel targets of the sP or iP during aggregate or cytokine stimulation, immunoprecipitations of such targets can be done to determine if this regulation is done directly with proteasome binding.

What is more, to better understand how these mechanisms are involved in diseases, it would be more relevant to investigate these observations in a more pathological setting, such as in the sP and iP-fluorescently tagged iPSC-derived microglia harbouring a synucleinopathy that are currently being established by the rest of lab.

Being able to target the iP as the cause of inflammation without affecting sP activity would be ground-breaking to reduce toxic side effects. The goal of this research is to uncover novel targets for therapies to impede neuroinflammation, and effectively treat a broad range of neurodegenerative disorders that arise due to overactive glial cells. Current drugs for AD and PD only help in reducing and controlling behavioral symptoms without addressing the cause of degeneration. Moreover, evidence suggests that prolonged usage of Levodopa, Parkinson's disease most common treatment, increases toxicity and inflammatory responses[69]. There is therefore an urgency to find ways of targeting the underlying problems of neuropathologies.

Bibliography

1. Babcock, K.R., Page, J.S., Fallon. J.R. & Webb, A.E. Adult Hippocampal Neurogenesis in Aging and Alzheimer's Disease. Stem *Cell Reports*. 16, 681-691 (2021).

2. Braak, H., Alafuzoff, I., Arzberger, T., Kretzschmar, H., & Del Tredici, K. Stageing of Alzheimer disease-associated neurofribrillary pathology using paraffin sections and immunohistochemistry. *Acta Neuropatho.* (4), 389-404 (2006).

3. Grosch, J., Winkler, J. & Kohl, Z. Early Degeneration of Both Dopaminergic and Serotonergic Axons - A common Mechanism in Parkinson's Disease. Front. in Cell. Neurosci. doi.org/10.3389/fncel.2016.00293 (2016).

4. Goedert, M. Alzheimer’s and Parkinson’s diseases: The prion concept in relation to assembled Aβ, tau, and α-synuclein. Science (80-.). 349, 61–69 (2015).

5. Thibauseau, T.A., Anderson, R.T & Smith, D. M. A common mechanism of proteasome impairment by neurodegenerative disease-associated oligomer. Nature Communications 9 (2018).

6. Kayed, R. & Lasagna-Reeves, C. A. Molecular Mechanisms of amyloid oligomers toxicity. J. Alzheimer's Dis. 3, 67-78 (2012).

7. Furcila, D., Dominguez-Alvaro, M., DeFelipe, J., & Alonso-Nanclares, L. Subregional Density of Neurons, Neurofribillary Tangles and Amyloid Plaques in the Hippocampus of Patients With Alzheimer's Disease. Front. Neuroanat. DOI: 10.3389/.2019.00099 (2019).

8. Hill. E, Gowers, R., Richardson, M. J. E. & Wall M. J. α-Synuclein Aggregates Increase the Conductance of Substancia Nigra Dopamine Neurons, an Effect Partly Reversed by the KATP Channel Inhibitor Glibenclamide. eNeuro. 8, 0330-20.2020 (2020).

9. Wang, S., Chu, C., Stewart T., Ginghina C., Wang Y., Nie H., Guo M., Wilson B., Hong, J. & Zhang, J. α-Synuclein, a chemoattractant, directs microglial migration via H2O2-dependent Lyn phosphorylation. Proc Natl Acad Sci USA 112 (15), E1926-E1935 (2015).

10. Glass, KC., Saijo, K., Winner, B., Marchetto, MC. & Gage, FH. Mechanisms underlying inflammation in neurodegeneration. Cell 6, 140 (2010).

11. GlaRamesh, G., MacLean, AG. & Philipp, MT. Cytokines and chemokines at the crossroads of neuroinflammation, neurodegeneration, and neuropathic pain. Mediators Inflamm DOI: 10.1155/2013/480739 (2013).

12. Rostami, J., Mothes, T., Kolahdouzan, M., Eriksson, O., Moslem, M., Bergstrom, J., Ingelsson, M., O'Callaghan, P., Healey, L. M., Falk, A. & Erlandsson, A. Crosstalk between astrocytes and microglia results in increased degradation of α-synuclein and amyloid-β aggregates. J Neuroinflammation 18(1) 124- (2021).

13. Majerova, P., Zilkova, M., Kazmerova, Z., Kovac, A., Paholikova, K., Kovacech, B., Zilka, N. & Novak, M. Microglia display modest phagocytic capacity for extracellular tau oligomers. Journal of Neuroinflammation 11, 161 (2014).

14. Damisah, E. C., Hill, R. A., Rai, A., Chen, F., Rothlin, C. V., Ghosh, S. & Grutzendler, J. Astrocytes and microglia play orchestrated roles and respect phagocytic territories during neuronal corpse removal in vivo. Cellular Neuroscience 6 (2020).

15. Joshi, P., Turola, E., Ruiz, A., Bergami, A., Libera, D. D., Benussi, L., Giussani, P., Magnani, G., Comi, G., Legname, G., Ghidoni, R., Furlan, R., Matteoli, M. & Verderio, C. Microglia convert aggregated amyloid-β into neurotoxic forms through the shedding of microvesicles. Cell Death & Differentiation 21, 582-593 (2014).

16. González-Reyes, R. E., Nava-Mesa, M. O., Vargas-Sánchez, K., Ariza-Salamanca, D. & Mora-Muñoz, L. Involvement of astrocytes in Alzheimer's disease from a neuroinflammatory and oxidative stress perspective. Front. Mol. Neurosci. 10, 1–20 (2017).

17. Vainchtein, I. D. & Molofsky, A. V. Astrocytes and Microglia: In Sickness and in Health.Trends Neurosci. 43, 144–154 (2020).

18. Salter, M. W. & Stevens, B. Microglia emerge as central players in brain disease. Nat. Med. 23, 1018–1027 (2017).

19. Phatnani, H. & Maniatis, T. Astrocytes in neurodegenerative disease. Cold Spring Harb. Perspect. Biol. 7, 1–18 (2015).

20. Skaper SD., Giusti P. & Facci L. Microglia and mast cells: two tracks on the road to neuroinflammation. FASEB J 26(8):3103–17 (2012).

21. Amor, S., Puentes, F., Baker, D. & van der Valk, P. Inflammation in neurodegenerative diseases. Immunology 129(2): 154-69 (2010).

22. Chitnis, T. & Winer, HL. CNS inflammation and neurodegeneration. J Clin Invest 127(10): 3577-3587 (2017).

23. Kwon, HS. & Seong-Ho, K. Neuroinflammation in neurodegenerative disorders: the roles of microglia and astrocytes. Transl Neurodegener 9(1):42 (2020).

24. Stephenson, J., Nutma, E., van der Valk, P. & Amor, S. Inflammation in CNS neurodegenerative diseases. Immunology 154, 204–219 (2018).

25. Wagner, L. K. et al. Immunoproteasome deficiency alters microglial cytokine response and improves cognitive deficits in Alzheimer's disease-like APPPS1 mice. Acta Neuropathol. Commun. 5, 52 (2017).

26. Strohmeyer, R., Shelton, J., Lougheed, C. & Breitkopf, T. CCAAT-Enhancer Binding Protein- β Expression and Elevation in Alzheimer's Disease and Microglial Cell Cultures. PLoS One 9 e88617 (2014).

27. Wang, H., Liu, X., Chen, S. & Ye, K. Spatiotemporal activation of the C/EBP β/δ-secretase axis regulates the pathogenesis of Alzheimer's disease. PNAS 115 E12427-E12434 (2018).

28. Chen, C., Zhou, W., Liu, S., Deng, Y., Cai, F.C., Tone, M., Tone, Y., Tong, Y. & Song, W. Increased NF-κ signalling up-regulates BACE1 expression and its therapeutic potential in Alzheimer's disease. International Journal of Neuropsychopharmacology 15 77-90 (2012).

29. Nijboer, C.H.A., Heiinen C.J., Groenendaal, F., May, M.J., van Bel, F. & Kavelaars, A. Strong Neuroprotection by Inhibition of NF-κB After Neonatal Hypoxia-Ischemia Involves Apoptotic Mechanisms but Is Independent of Cytokines. Stroke 39 2129-2137 (2008).

30. Morales-Garcia, J.A., Gine, E., Hernandez-Encina, E., Aguilar-Morante, D., Sierra-Magro, A., Sanz-SanCristobal, M., Alsonso-Gil, S., Sanchez-Lanzas, R., Castano, J.G., Santons, A. & Perez-Castillo, A. CCAAT/Enhancer binding protein β silencing mitigates glial activation and neurodegeneration in a rat model of Parkinson's disease. Scientific

Reports 7 13526 (2017).

31. De, S. et al. Different soluble aggregates of Aβ42 can give rise to cellular toxicity through different mechanisms. Nat. Commun. 10, (2019).

32. Ferrington, D. A. & Gregerson, D. S. Immunoproteasomes: Structure, function, and antigen presentation. Progress in Molecular Biology and Translational Science vol. 109 (2012).

33. Moritz, K. E. et al. The role of the immunoproteasome in interferon-γ-mediated microglial activation. Sci. Rep. 7, 1–16 (2017).

34. McBerry, C., Gonzalez, R. M. S., Shryock, N., Dias, A. & Aliberti, J. SOCS2-induced proteasome-dependent TRAF6 degradation: A common anti-inflammatory pathway for control of innate immune responses. PLoS One 7, (2012).

35. McCarthy, M. K. & Weinberg, J. B. The immunoproteasome and viral infection: A complex regulator of inflammation. Front. Microbiol. 6, 1–16 (2015).

36. Ugras, S. et al. Induction of the Immunoproteasome Subunit Lmp7 Links Proteostasis and Immunity in α-Synuclein Aggregation Disorders.EBioMedicine 31,307–319 (2018).

37. Lundh, M. et al. The immunoproteasome is induced by cytokines and regulates apoptosis in human islets. J. Endocrinol. 233, 369–379 (2017).

38. Murata, S. et al. Immunoproteasome assembly and antigen presentation in mice lacking both PA28α and PA28β. EMBO J. 20, 5898–5907 (2001).

39. Hallermalm, K. et al. Tumor necrosis factor-α induces coordinated changes in major histocompatibility class I presentation pathway, resulting in increased stability of class I complexes at the cell surface. Blood 98, 1108–1115 (2001).

40. Orre, M. et al. Reactive glia show increased immunoproteasome activity in Alzheimer's disease. Brain 136, 1415–1431 (2013).

41. Cascio, P., Call, M., Petre, B.M., Walz, T. & Goldberg A.L. Properties of the hybrid form of the 26S proteasome containing both 19S and PA28 complexes. EMBO J 21 2636-2645 (2002).

42. Karmon, O. & Aroya, A.B. Spatial Organization of Proteasome Aggregates in the Regulation of Proteasome Homeostasis. Front. Mol. Biosci. doi.org/10.3389/fmolb.2019.00150 (2020).

43. Cliffe, R., Sang, J.C., Kundel, F., Finley, D., Klenerman, D. & Ye, Y. Filamentous Aggregates Are Fragmented by the Proteasome Holoenzyme. Cell Reports 26 2140-2149 (2019).

44. Ye, Y., Klenerman, D. & Finley, D. N-Terminal Ubiquitination of Amyloidogenic Proteins Triggers Removal of Their Oligomers by the Proteasome Holoenzyme. J Mol Biol 432 585- 596 (2020).

45. Guo, T., Liu, C., Yang, C., Wu, J., Su, P. & Chen, J. Immunoproteasome subunit PSMB8 regulates microglia-mediated neuroinflammation upon manganese exposure by PERK signaling. Food Chem Toxicol 163:112951 DOI: 10.1016/j.fct.2022.112951 (2022).

46. French, T., Israel, N., Dusedau, HP., Tersteegen, A., Steffen, J., Cammann, C., Topfstedt, E., Dieterich, D., Schuler, T., Seifert, U. & Dunay, IR. The Immunoproteasome Subunits LMP2, LMP7 and MECL-1 Are Crucial Along the Induction of Cerebral Toxoplasmosis. Front Immunol 12:619465 DOI: 10.3389/fimmu.2021.619465 (2021).

47. Zalocusky, KA., Najm, R., Taubes, AL., Hao, Y., Yoon, SY., Koutsodendris, N., Nelson, MR., Rao, A., Bennett, DA., Bant, J., Amornkul, D., Xu, Q., An, A., Cisne-Thomson, O. & Huang, Y. Neuronal ApoE Upregulates MHC-I Expression to Drive Selective Neurodegeneration in Alzheimer's Disease. Nat Neurosci 14(6): 786-798 (2021).

48. Jimenez-Ferrer, I, Backstrom, F., Duenas-Rey, A., Jewett, M., Boza-Serrano, A., Luk, KC., Deierborg, T. & Swanberg, M. The MHC class II transactivator modulates seeded alpha-synuclein pathology and dopaminergic neurodegeneration in an in vivo rat model of Parkinson's disease. Brain Behav Immun 91:369-382 (2021).

49. Wang L. & Wei X. T Cell-Mediated Autoimmunity in Glaucoma Neurodegeneration. Front Immunol 16: 803485 DOI: 10.3389/fimmu.2021.803485 (2021).

50. Williams, GP., Schonhoff, AM., Jurkuvenaite, A., Gallups, NJ., Standaert, DG. & Harms, AS. CD4 T cells mediate brain inflammation and neurodegeneration in a mouse model of Parkinson's disease. Brain 144(7) (2021).

51. Chen, X., Zhang, X., Wang, Y., Lei, H., Su, H., Zeing, J., Pei, Z. & Huang, R. Inhibition of immunoproteasome reduces infarction volume and attenuates inflammatory reaction in a rat model of ischemic stroke. Cell Death Dis 6(1):e1626 (2015).

52. Chen, X., Wang, Y., Yap, N. & Lin, Z. Immunoproteasome modulates NLRP3 inflammasome-mediated neuroinflammation under cerebral ischaemia and reperfusion conditions. J Cell Mol Med 26(2):462-474 (2022).

53. Guo, T., Liu, C., Yang, C., Wu, J., Su, P. & Chen, J. Immunoproteasome subunit PSMB8 regulates microglia-mediated neuroinflammation upon manganese exposure by PERK signaling. Food Chem Toxicol 163:112951 DOI:10.1016/j.fct.2022.112951 (2022).

54. Ibrahim, RR., El-Esawy, RO. & El-Sakaa, MH. Troxerutin downregulates C/EBP-β gene expression via modulating the IFNγ-ERK1/2 signaling pathway to ameliorate rotenone-induced retinal neurodegeneration. J Biochem Mol Toxicol 34(6):e22482 (2020).

55. Maranto, J., Rappaport, J. & Datta, PK. Role of C/EBP-β, p38 MAPK, and MKK6 in IL-1β-mediated C3 gene regulation in astrocytes. J Cell Biochem 112(4)1168-75 (2011).

56. Ndoja, A., Reja, R., Lee, S., Webster, JD., Ngu, H., Rose, CM., Kirkpatrick, DS., Modrusan, Z., Chen, YJ., Dugger, DL., Gandham, V., Xie, L., Newton, K. & Dixit, VM. Ubiquitin Ligase COP1 Suppresses Neuroinflammation by Degrading c/EBPβ in Microglia. Cell 182(5):1156-1169 (2020).

57. Hattori, T., Ohoka, N., Inoue, Y., Hayashi, H. & Onozaki, K. C/EBP family transcription factors are degraded by the proteasome but stabilized by forming dimer. Oncogene 22:1273-1280 (2003).

58. Ran, F.A, Hsu, P.D., Wright, J., Agarwala, V., Scot, D.A. & Zhang, F. Genome engineering using the CRISPR-Cas9 system. Nature Protocols 8 2281-2308 (2013).

59. Haenseler, W., Sanson, A.N., Buchrieser, J., Newey, S.E., Moore, C.S., Nicholls, F.J., Chintawar, S., Schnell, C., Antel, J.P., Allen, N.D., Cader, M.Z., Wade-Martins, R., James, W.S. & Cowley, S.A. A Highly Efficient Human Pluripotent Stem Cell Microglia Model Displays a Neuronal-Co-culture-Specific Expression Profile and Inflammatory Response. Stem Cell Reports 8 1727-1742 (2017).

60. Roelofs, J., Suppahia, A., Waite, K.A. & Park, S. Native Gel Approaches in Studying

Proteasome Assembly and Chaperones. Springer Nature Protocols DOI:10.1007/978-1-4939- 8706-1_16 (2018).

61. Schindelin, J., Arganda-Carreras, I., Frise, E., Kaynig, V., Longair, M., Pietzsch, T., Cardona, A. Fiji: an open-source platform for biological-image analysis. Nature Methods, 9(7), 676–682 (2012).

62. Yasuda, S., Tsuchiya, H., Kaiho, A., Guo, Q., Ikeuchi, K., Endo, A., Arai, N., Ohtake, F., Murata, S., Inada, T., Baumeister, W., Fernandez-Busnadiego, R., Tanaka, K. & Saeki, Y. Stress-and ubiquitilation-dependent phase separation of the proteasome. Nature 578 296-300 (2020).

63. Wang, B., Zhang, L., Dai, T., Qin, Z., Lu, H., Zhang, L. & Zhou, F. Liquid–liquid phase separation in human health and diseases. Signal Transduct Target Ther 6(1): 290 (2021).

64. Cohen-Kaplan, V., Livneh, I. & Ciechanover, A.,Proteasome phase separation: a novel layer of quality control. Cell Res 30(5):374-375 (2020).

65. Zhang, L., Gurskaya, NG., Marzlyal, EM., Staroverov, DB., Mudrik, NN., Samarkina, ON., Vinokurov, LM., Lukyanov, S. & Lukyanov, KA. Method for real-time monitoring of protein degradation at the single cell level. Biotechniques 42(4):446,448, 450 (2007).

66. Hamer, G., Matilainen, O. & Holmberg, C.I. A photoconvertible reporter of ubiquitin-proteasome system in vivo. Nat Methods 7 473-7 (2010).

67. Tanaka, K. The proteasome: Overview of structure and function. Proc Jpn Acad Ser B Phys Biol Sci 85 12-34 (2009).

68. Wang, C., Li, C., Hsu, H., Cho, C., Yen, M., Weng, T., Chen, W., Hung, M., Lee, K., Chen, Y. & Lai, M. PSMB5 plays a dual role in cancer development and immunosuppression. Am J Cancer Res 7 2103-2120 (2017).

69. D orszewska, J., Prendecki, M., Lianeri, M. & Kozubski, W. Molecular Effects of L-dopa Therapy in Parkinson's Disease. Curr. Genomics 15, 11–17 (2014).

Appendix

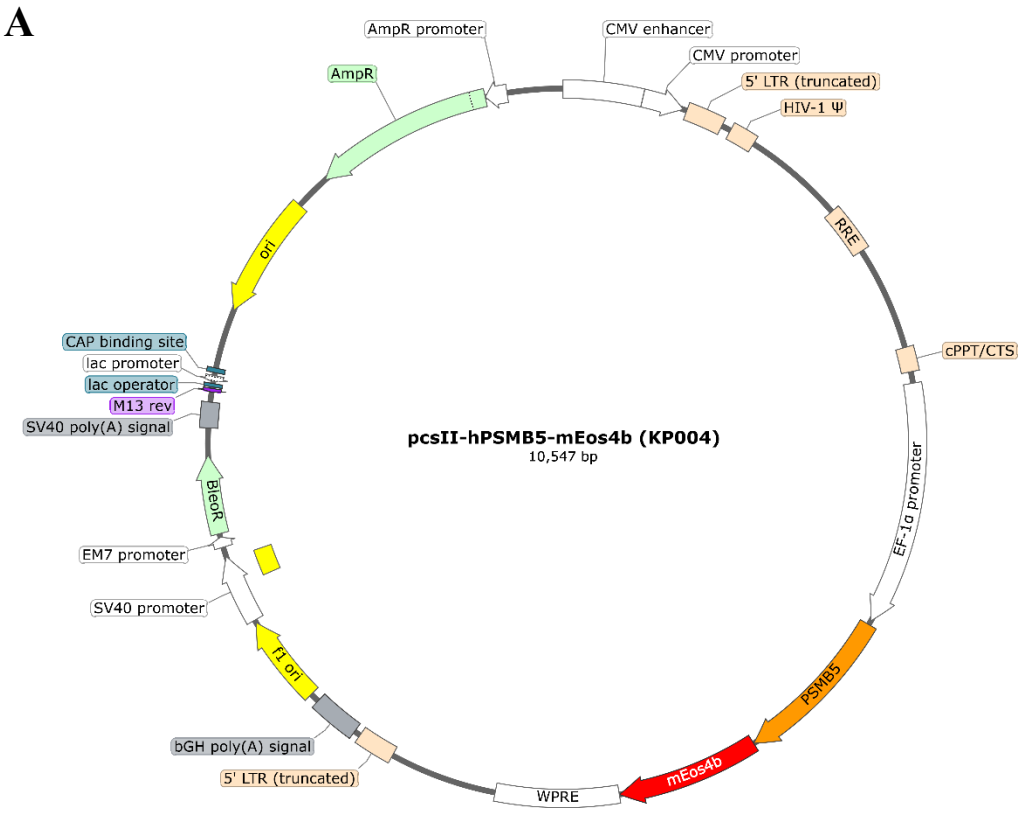

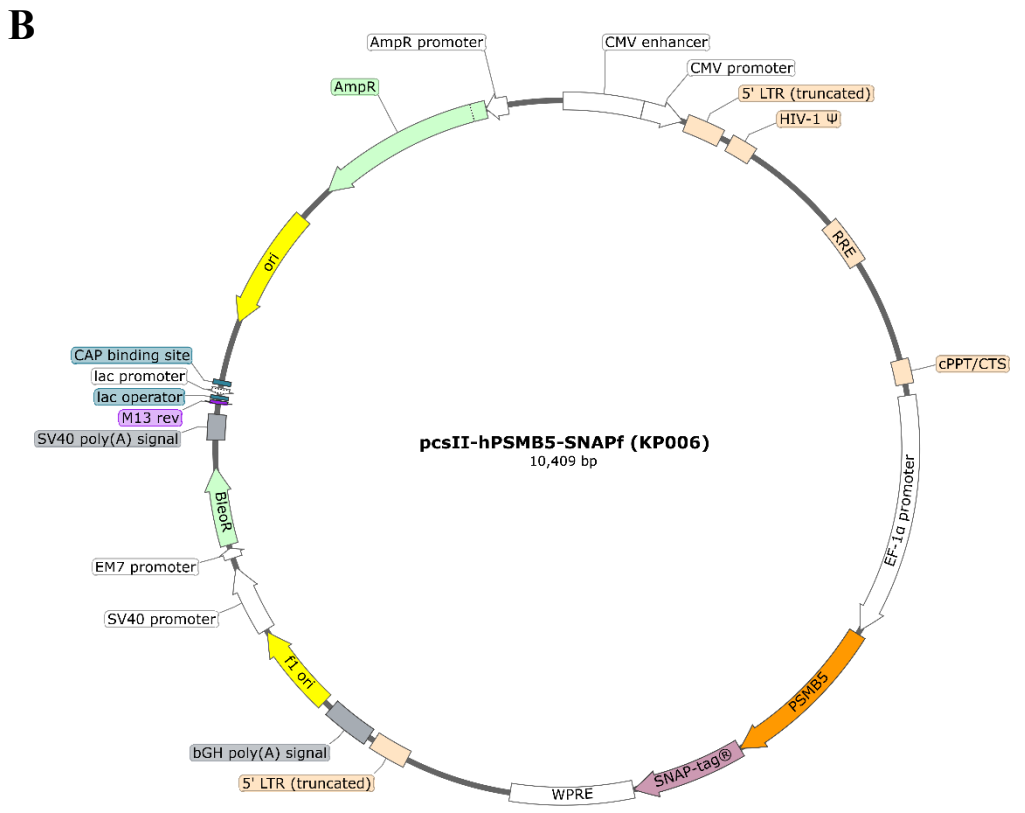

Appendix Figure A1. Map of pcsII-hβ5-FP. A pcsII-hβ5-mEos4b **B** pcsII-hβ5-SNAP.

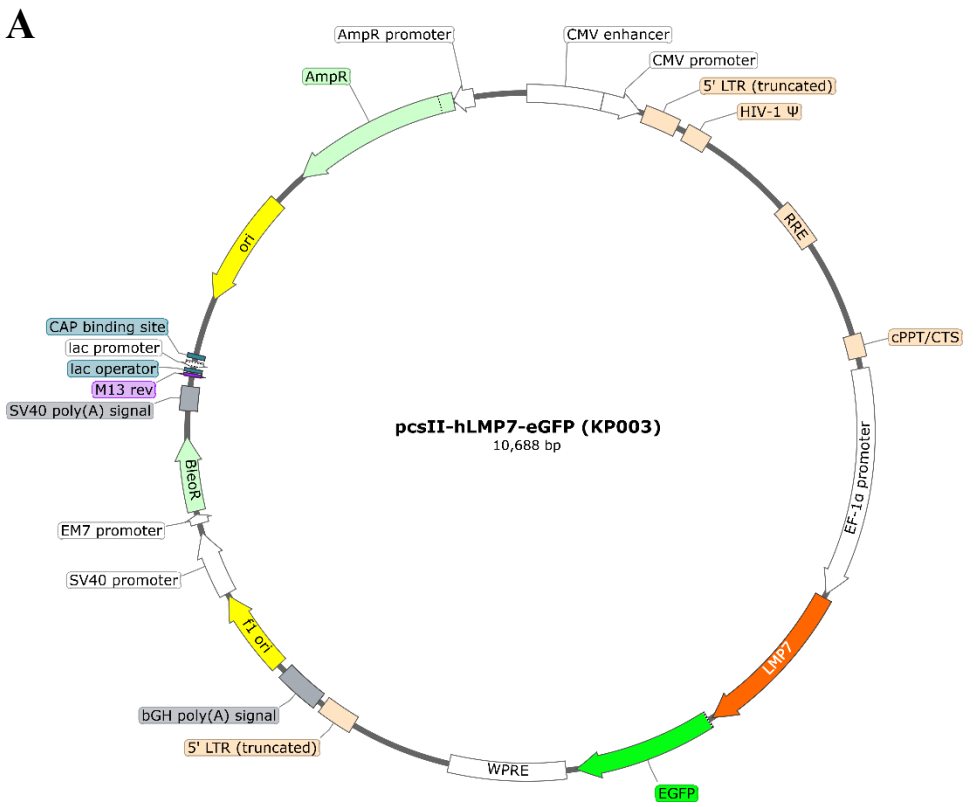

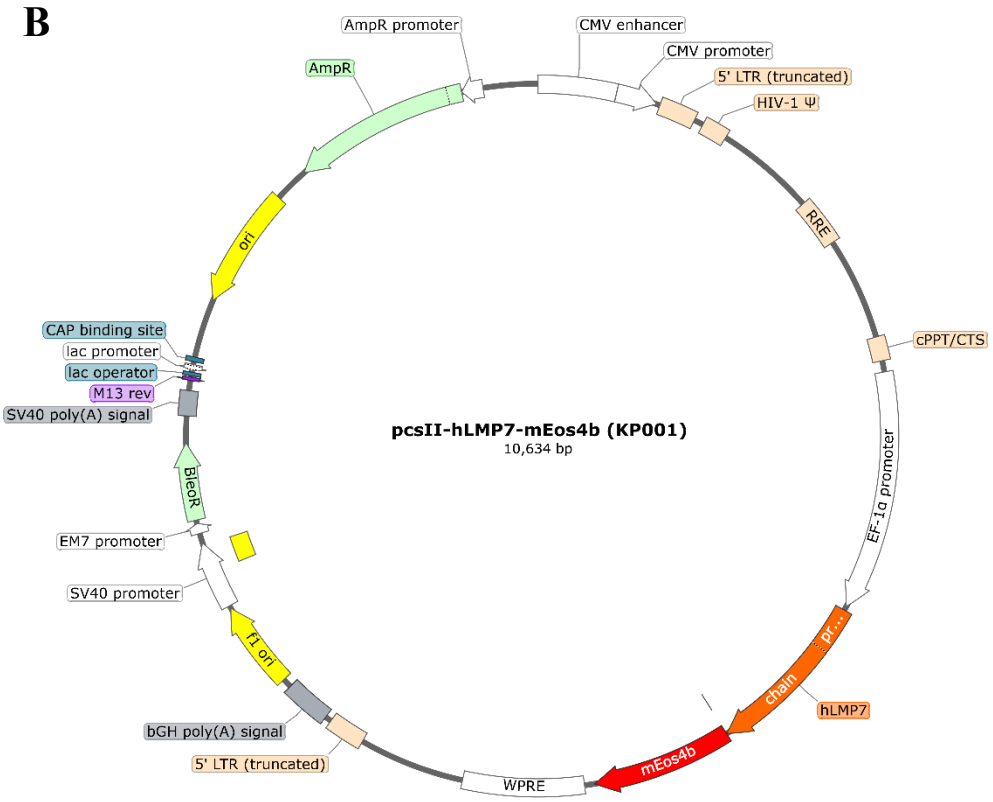

Appendix Figure A2. Map of pcsII-hβ$_{5i}$-FP. A pcsII-hβ$_{5i}$-mEos4b **B** pcsII-hβ$_{5i}$-eGFP.

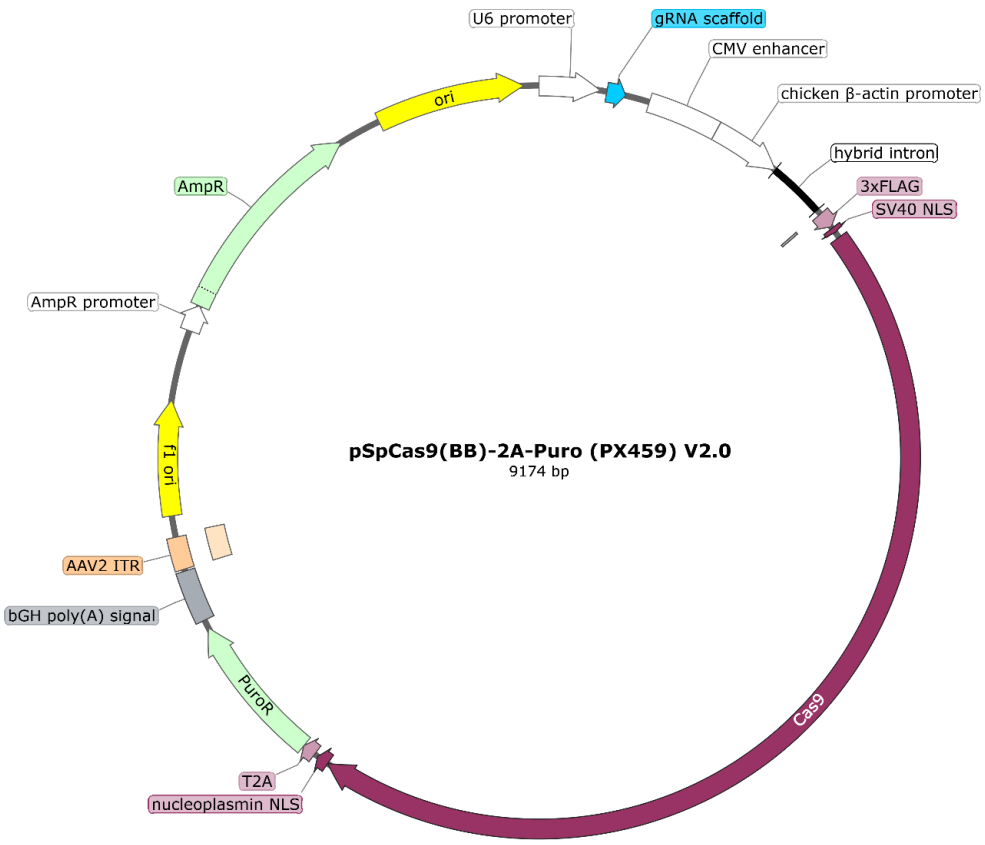

Appendix Figure A3. Map of Cas9 plasmid.